ORIGINAL PAPER

Flight dynamics and control assessment for differential thrust aircraft in engine inoperative conditions including aero-propulsive effects

Maurice F. M. Hoogreef[1] · **Johannes S. E. Soikkeli[2]**

Abstract

Differential thrust can be used for directional control on distributed electric propulsion aircraft. This paper presents an assessment of flight dynamics and control under engine inoperative conditions at minimum control speed for a typical distributed propulsion aircraft employing differential thrust. A methodology consisting of an aerodynamic data acquisition module and a non-linear six-degrees-of-freedom flight dynamics model is proposed. Directional control is achieved using a controller to generate a yaw command, which is distributed to the propulsors through a thrust mapping approach. A modified version of the NASA X-57 aircraft is selected for case studies, where the engine inoperative condition is considered to impact the three leftmost propulsors during climb at minimum control speed. The objective also includes the assessment of the impact of the aero-propulsive coupling for such an aircraft during a failure case. Results show that during the recovery manoeuvre, the aircraft experiences a 78% reduction in total thrust and 30% reduction in total lift caused by the aggressive yaw control effort required to control the heading of the aircraft. Consequently, the powered-stall speed is increased, and the aircraft temporarily loses altitude during the recovery manoeuvre. Differential thrust provides sufficient yaw authority during the engine inoperative condition, and is, therefore, seen to potentially replace the functionality of the rudder for the climb condition that was studied. Additionally, reduction of the vertical tail area was explored and seen to be possible if the response time of the system is low enough. For the studied configuration, this required a response within 400 ms for reduced vertical tail areas.

Keywords Differential thrust · Distributed electric propulsion · Directional control · Aero-propulsive effects · Engine inoperative conditions

List of symbols
Latin symbols

$C_{[]_{[]}}$	Force coefficient (~)
$C_{M_{[]}}^{[]}$	Moment coefficient (~)
C_{T}	Thrust Coefficient $\frac{T}{\rho \cdot n^2 \cdot d^4}$ (~)
D	Drag (N)
d	Propeller diameter (m)
$\boldsymbol{F}$	Force vector in body frame (N)
$\boldsymbol{H}$	Angular momentum vector in body frame (kg m²/s)
$\boldsymbol{I}$	Aircraft inertia matrix in body frame (kg m²)
I_{prop}	Propeller inertia in rotation axis (kg m²)
I_x, I_y, I_z	Aircraft moments of inertia in body frame (kg m²)
I_{xy}, I_{xz}, I_{yz}	Aircraft products of inertia in body frame (kg m²)
$\boldsymbol{i}$	Propeller rotation axis unit vector in body frame (~)
J	Advance ratio (~)
L	Lift (N)
$\boldsymbol{M}$	Moment vector in body frame (Nm)
m	Aircraft mass (kg)
n	Propeller rotational speed (rad/s)
P	Power (W)
p, q, r	Angular velocity vector components in body frame (rad/s)
T	Thrust (N)
t	Time (s)
u, v, w	Velocity vector components in body frame (m/s)
V_∞	Freestream velocity (m/s)
$\boldsymbol{V}$	Velocity vector in body frame (m/s)

✉ Maurice F. M. Hoogreef
m.f.m.hoogreef@tudelft.nl

1 Flight Performance and Propulsion Section, Faculty of Aerospace Engineering, Delft University of Technology, 2629 HS Delft, The Netherlands

2 Pipistrel Vertical Solutions, Ajdovščina, Slovenia

| W | Weight (N) |
| x, y, z | Coordinate axes (~) |

Greek symbols

α	Angle of attack (deg)
β	Side-slip angle (deg)
γ	Flightpath angle (deg)
δ	Control surface deflection angle (deg)
θ	Pitch angle (deg)
ρ	Density (kg/m^3)
φ	Bank angle (deg)
Ψ	Yaw command $\Psi \in [0, 1]$ (~)
ψ	Yaw angle (deg)
$\boldsymbol{\Omega}$	Angular velocity vector (rad/s)
ω	Angular velocity (rad/s)

Superscripts

A	Airframe
C	Control surface
G	Gravity
P	Aero-propulsive
*	Deformation
$\cdot$	Rate of change (1/s)

Subscripts

B,E,V,W	In body, Earth, vertical or wind frame
F,M	Due force or moment vector in body frame
L,D	Due lift or drag in wind frame
T,Q	Due thrust or torque in propeller axis
a,e,r	Due aileron, elevator, rudder
p,q,r	Due angular velocity in body frame; roll, pitch, yaw
x, y, z	In coordinate axes
0	Due airframe only
i, 1..6	Due propeller 1..6

Abbreviations

CAD	Computer-aided design
CFD	Computational fluid dynamics
CS-23	Certification specifications Part 23 for Normal, Utility, Aerobatic and Commuter Aeroplanes
EASA	European Union Aviation Safety Agency
NASA	National Aeronautics and Space Administration
PID	Proportional integral derivative
RANS	Reynolds-averaged Navier–Stokes
RPM	Revolutions per minute
RSM	Response surface methodology
TLAR	Top-level aircraft requirement

1 Introduction

Distributed electric propulsion concepts have been envisaged as a promising solution to meet the Flightpath 2050 environmental goals set by, for example, the Air Transport Action Group[1] or the European Commission in its Flightpath 2050 vision on aviation [1] to address modern-day aviation's climate impact. Significant research has been performed aimed at exploiting potential synergistic benefits between distributed propulsion and (hybrid) electric powertrains (e.g. [2–14]). The recent release of the Strategic Research and Innovation Agenda for the proposed European Partnership for Clean Aviation [15] has set distributed electric propulsion as a key innovation, setting the stage for further research.

Electric engines are mostly scale independent, compared to turbine engines whose efficiency and power-to-weight ratio suffer significantly when scaled down [16]. Therefore, it is possible to divide the propulsion into multiple smaller electric engines. Moreover, electric engines can be decoupled from the energy storage/production devices, and hence multiple smaller electric engines can be distributed into unconventional locations, improving the performance over more conventional designs through synergistic aero-propulsive effects. Additionally, distributed propulsion can be leveraged to enable new capabilities in vehicle control.

In the case of leading edge mounted distributed propulsion, an array of propulsors is mounted along the span of the wing in front of the leading edge. A notional example of the configuration studied in this article is presented in Fig. 1. The propulsors (1..n) increase the dynamic pressure over the wing (B) in the areas washed by the propeller slipstreams, hence increasing the lift generated by the wing. This phenomenon is herein referred to as power augmented lift. Additionally, the maximum lift coefficient is also increased allowing for designs with reduced wing surface area, as was for example demonstrated by Stoll et al. [17].

Distributed propulsion can be used beneficially from a control and stability point-of-view. Most importantly, the size of a vertical tail (D) could be reduced or eliminated entirely. This would remove the drag caused by the vertical tail and also decrease the weight of the aircraft. According to Schiltgen and Freeman [18] this could be achieved in two ways. First, by either designing fault-tolerant distributed propulsion which would reduce or eliminate the worst-case adverse yaw failure modes. Second, the distributed propulsion could be used for active differential thrust control, which could lower the rudder's yaw requirements. The latter was also shown in the simulations by Wortmann

Fig. 1 Illustration of the aircraft configuration under consideration, with fuselage (A), wing (B) with "*n*" distributed propulsors along the leading edge, horizontal stabiliser (C) and vertical stabiliser (D) (model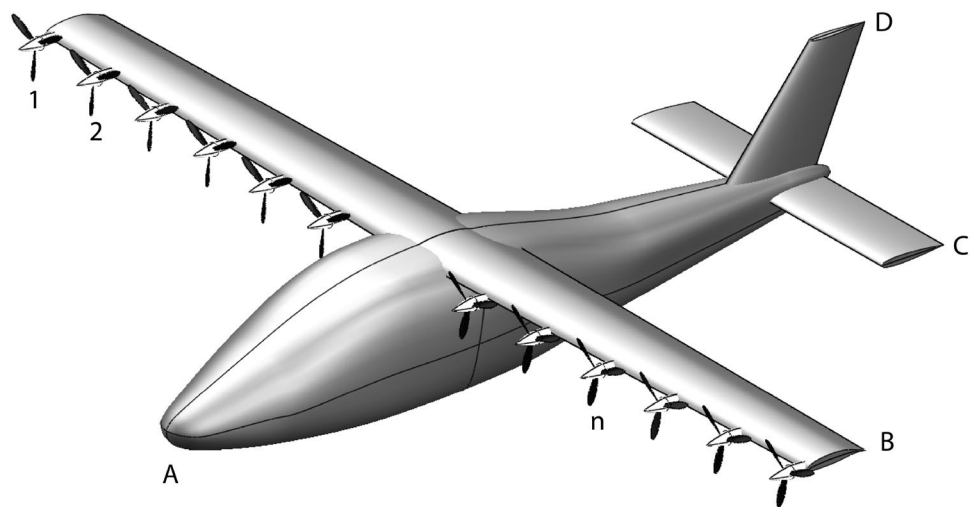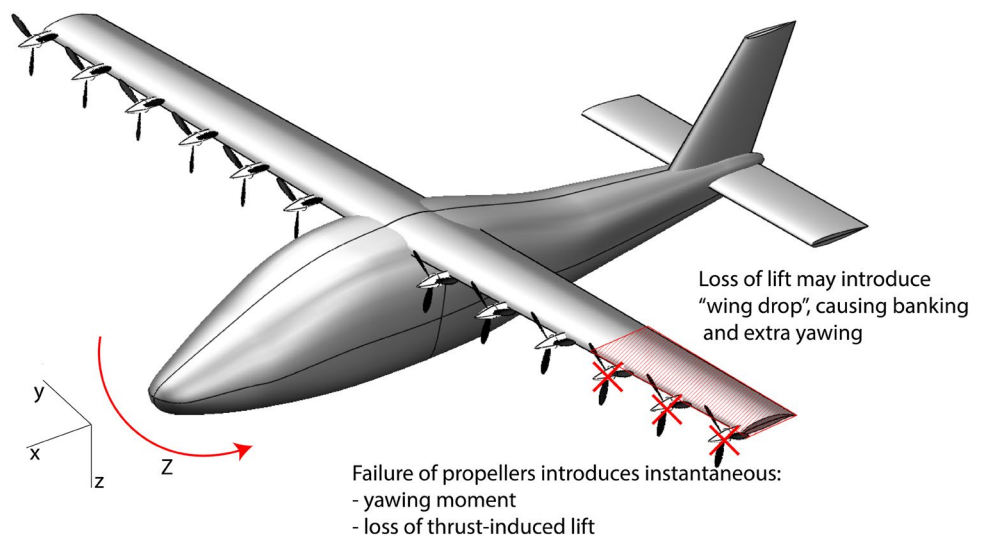 adjusted from X-57 Maxwell Open-VSP model, available at http://hangar.openvsp.org/vspfiles/414; visited 27 October 2020)

Fig. 2 Illustration of effects induced by engine inoperative conditions, exaggerated for the loss of three propulsors on the same wing

Loss of lift may introduce "wing drop", causing banking and extra yawing

Failure of propellers introduces instantaneous:
- yawing moment
- loss of thrust-induced lift

[19] and is possible thanks to electric motors having a short response time due to high torque combined with small inertia. It should be noted though that active yaw control through differential thrust is likely a requirement when vertical stabiliser/rudder are reduced/removed. Additionally, electrical motors are usually rated for short-term burst power,[2] which is often higher than the maximum continuous power. The burst power could be used for the operative engines in a engine-inoperative scenario to reduce the adverse yaw [20]. Wortmann [19] suggests that integrating yaw control into the distributed propulsion system could remove the rudder deflection hardware, which would lead to beneficial weight reduction. However, Wortmann also highlights that distributed propulsion complicates engine-inoperative conditions and increases the number of possible failure scenarios.

Since propulsion must, in the case of Fig. 1, provide both directional control, thrust and lift control, new challenges arise in situations where those two requirements are competing. Such a situation is presented by engine inoperative conditions during climb at minimum control speed, because for differential thrust aircraft, the propulsion must provide enough thrust while countering the adverse yawing moment. Additionally, for an aircraft that relies on power augmented lift, the condition is further aggravated by lift degradation due to failed propulsors and required directional control effort. To evaluate the envisaged benefits of differential thrust, the engine inoperative condition of such aircraft must be considered as important design constraint. This is illustrated in Fig. 2.

Various studies have been performed regarding the stability and control of differential thrust configurations. In his

---

[2] Consider for example the overloading explained by the US Department of Energy in https://www.energy.gov/sites/prod/files/2014/04/f15/10097517.pdf, visited 20 October 2020.

simulations, Wortmann [19] investigated the differential thrust of fixed wing aircraft at take-off conditions with minimum control speed using a state-space model. A Tecnam P2006T with varying number of leading edge propulsors from 2 to 18 was used to study climb performance relating to certification requirements of light aircraft (CS-23). Yaw control is achieved only through differential thrust and it is assumed that the electric motors can provide a burst power of 2 times the maximum continuous power. The control law is set as such that all engines on one wing operate at the same thrust level. Wortmann [19] concludes that when 4 or more propulsors are present on the aircraft, it can cope with the requirements for yaw control. However, the dissertation also importantly notes there is a risk that both the power requirement and the yaw control cannot be satisfied at the same time in all conditions. In those cases, Wortmann [19] chose to satisfy the yaw control over power requirement. It was demonstrated that for an aircraft with 6 propulsors, the failure of both outermost propulsors led to the aircraft not being able to satisfy the climb requirement. In another study, Wortmann [19] also notes that for aircraft with 12 propulsors, the aircraft can satisfy the requirements for up to three outermost propulsors inoperative. However, all these studies were performed without considering the aero-propulsive interactions. As such, high-lift conditions (such as minimum control speed) where the lift generation is dependent on the propulsors as well, can be even more critical.

Similarly, Freeman and Klunk [21] investigated whether differential thrust could provide similar response to that of a rudder using state-space simulation model and compared this to test data, also without direct aero-propulsive interactions. In the article by Klunk et al. [22], the reduction of the vertical tail for the ECO-150 vehicle from a conceptual design standpoint was investigated. The study by Freeman and Klunk [21] relies on a vortex lattice solver (VSPAERO) to estimate the parasite drag and stability and control derivatives. However, it did not include the distributed propulsion effects in the aerodynamic analysis (only lifting surfaces are analysed) but estimated their effects on the tail separately. The authors conclude that rudder deflection commands can be mimicked using asymmetric throttle commands that maintain constant net thrust. A recent study by Pfeifle et al. [23] investigates the use of differential thrust for yaw control on tip-mounted propeller aircraft and shows an application during flight tests. On both test beds their controller achieved coordinated flight and strong damping of the Dutch roll motion using differential thrust alone.

Nguyen Van et al. [24, 25] investigated differential thrust and vertical tail reduction through flight envelope and stability analysis, without aero-propulsive interactions or dynamic simulations. The main aim of these studies was to develop a methodology to size the vertical tailplane for reduced lateral static stability. An optimisation-based approach to minimise the installed power for the engine-inoperative scenario while maintaining the climb requirements was used, where the optimisation constraints contain the aircraft dynamics with an underlying assumption that the lateral coefficient of each component can be separable (wing, fuselage, vertical tail). A combination of a vortex lattice solver (VSPAERO) for wing and fuselage contributions and the vertical tail design, stability, and control (VeDSC) method, developed by Ciliberti et al. [26] for the vertical tail sizing and analysis. The latter relies on CFD to evaluate the effects of aerodynamic interference among airplane subparts, calculated as the ratio between static directional stability derivatives of aircraft configurations differing for one component (e.g. wing on versus wing off), for hundreds of combinations. This has been used to create reference charts with delta factors that can easily be applied in design. A recent article by Kou et al. [27] includes aero-propulsive effects through the VSPAERO toolkit provided through OpenVSP in the development of a model predictive control scheme for powered yaw control. Nguyen Van et al. [24, 25] conclude that differential thrust can maintain the control of the aircraft at low airspeed due to high control effectiveness and that oversized vertical tailplanes reduce the ability to achieve sideslip angles at high velocities. The latter is attributed to the large vertical tailplane providing large restoring moments and propulsors being easily saturated as power demand is higher. A later article by Nguyen Van et al. [28], investigated the sequential co-design of vertical tail and control laws for an aircraft actively using differential thrust, instead of a rudder. This led to the conclusion that replacement of an entire rudder for a typical turboprop aircraft by differential thrust is not recommended, as the electro motor bandwidth was shown to have the largest influence on control effort. The work, however, excludes aero-propulsive interactions, focusing on the co-design methodology.

Earlier studies have not considered aero-propulsive effects directly or exclude a (thorough) dynamic analysis of the engine inoperative conditions. As illustrated in Fig. 2, aero-propulsive effects on aerodynamic and stability/control derivatives are important to consider because of their direct influence. Moreover, dynamic analysis is required to study the ability of the aircraft to recover from a loss of propulsion. Therefore, this research proposes a framework that is suitable for the conceptual aircraft design phase for the preliminary assessment of flight dynamics for aircraft with distributed propulsion employing differential thrust, including aero-propulsive effects. The objective of this article is to provide an initial investigation into the coupled aero-propulsive effects on the flight dynamical behaviour of an aircraft with distributed propulsion in a failure case. The framework is used to study the impact on controllability due to a loss of the three most outboard propellers as a worst case scenario, considering also their direct influence

on the generated lift. The loss of three propellers is hypothesised for the abrupt failure of one propeller damaging its two neighbours, with the outboard ones having the largest moment arm to the aircraft center of gravity. The case studies are limited to minimum control speed climb and focus on aero-propulsive effects rather than development of an integrated flight controller.

This paper is structured into seven sections, starting with this introduction. Section 2 covers the methodology and framework requirements for assessing the controllability of a differential thrust aircraft including aero-propulsive interactions. The framework implementation is described in Sect. 3. Section 4 presents the validation and verification studies that were performed to assess the fidelity of the proposed framework implementation. Section 5 establishes the case study aircraft geometry, parameters, and discusses the case study setup. Section 6 presents results of studies performed to investigate the aero-propulsive effects on control of the aircraft under engine inoperative conditions and the opportunities for rudder removal (trading off control authority through propeller thrust with power-augmented lift), and vertical tailplane size reduction for aircraft with distributed electric propulsion. Finally, Sect. 7 presents the conclusions of the research. Part of this work is based on [29].

2 Methodology and framework description

The proposed methodology should be suitable for the conceptual design phase, where position and number of propulsors, as well as the aircraft geometry, are still variable. As such, a framework will be developed that provides sufficient detail whilst at the same time being usable and relatively fast. The developed approach is presented in this section and consists of an aerodynamic module (including aero-propulsive interactions) and a non-linear six-degrees-of-freedom flight dynamics model, in combination with aircraft and propeller geometry. The overall framework implementation will be discussed in Sect. 3 and is illustrated in Fig. 4.

2.1 Aircraft configuration and geometry generation

The conceptual design phase typically sees an aircraft evolve from a set of top-level aircraft requirements (TLAR) through a mass and balance estimation, initial wing and fuselage design and a performance estimation to a preliminary layout and geometry of the aircraft. Hence, a full detailed CAD geometry is not yet readily available, and the CAD geometry must be built as a rudimentary geometry model (consider the notional drawing in Fig. 1) based on airfoil profiles for wing (B, in Fig. 1) and tail surfaces (C and D), planform definitions (typically a result of constraint analysis in a wing loading—power loading diagram) and a fuselage

(A) constructed around the desired payload. The mass and geometry estimation, with resulting aircraft balance and inertia estimates are therefore suited for mid-fidelity analyses of the flight dynamics or aerodynamics. Another aspect of this conceptual stage is that the design can be subject to significant change, even in terms of topology (for example the addition of another propeller). Therefore, the approach should also be flexible enough and parametric to deal with a variety of input geometries and topologies. Similar to the airframe geometry, the propeller geometry may also not yet be available and actuator disk models are typical for analyses at this stage of the design.

2.2 Wing and propeller aerodynamics

A consequence of the rudimentary aircraft geometry is that full-fledged computational fluid dynamics (CFD) may be too computationally expensive. However, it is important that aero-propulsive interactions are captured to study consequences of lift-enhancing propellers. Hence, a trade-off between complexity, fidelity and runtime is required; both for the airframe aerodynamics and the propeller aerodynamics.

Distributed propulsion concepts show strong aero-propulsive interactions. The interaction effects are especially important for aircraft sizing as the synergistic benefits can improve the overall performance of the aircraft. Thus, these effects must be captured at early stages of the design process. For such applications, a combination between mid-fidelity design-order methods (such as blade element methods—BEM) and parametric subsonic flow solvers provides sufficient detail at acceptable computational costs. Typical mid-fidelity solvers, such as potential flow methods can include aero-propulsive interactions, for example through the application of an actuator disk model. However, it is important that the operating conditions of this propeller are representative (for example by providing the input data to an actuator disk model through a BEM analysis of a propeller).

To analyse the aircraft dynamic response of a vehicle with many distributed, lift-enhancing propellers, the flight dynamics model requires aerodynamic and inertia data of the entire airframe, including the effects of control surface deflections and those of the aero-propulsive interactions. Additionally, mid-fidelity aerodynamic solvers typically do require a basic 3D CAD aircraft geometry.

The coupled propeller wing aerodynamic interaction can be evaluated simultaneously, however, the evaluation of the interaction effects between multiple rotating propellers is computationally challenging to evaluate all at once. In a conceptual sizing framework, such analyses would have to be performed dozens, if not hundreds of times to evaluate both minor and major design changes. To speed up the process, a superposition principle can be used, similar to what is done
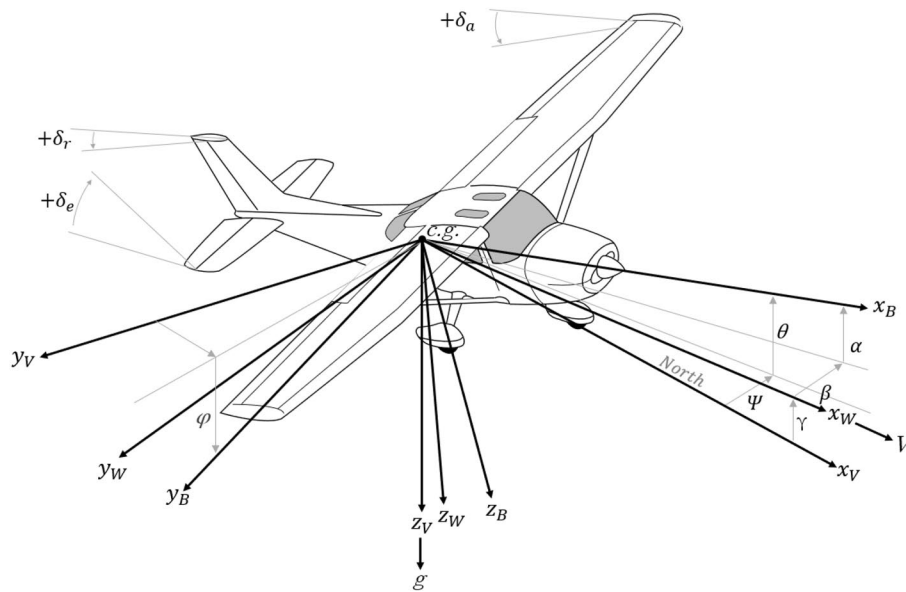
Fig. 3 Reference frame used in this paper

by Huber et al. [30], which captures dominant effects (but not all couplings and interactions) of neighbouring control surfaces. Since the goal is to evaluate the dominant impact of engine in-operative conditions at minimum control speed, for distributed propulsion aircraft, this approach is considered acceptable here as well. The actual impact of this decision will be evaluated.

2.3 Equations of motion

The flight dynamics can be modeled through a non-linear form of the six-degrees-of-freedom equations of motion. Here, the airframe is assumed to be rigid and with constant mass, the reference frame illustrated in Fig. 3 is used.

The Earth is assumed to be flat and non-rotating. Equations are according to Etkin [31]. The translational equations of motion in the body reference frame are then defined according to the forces due to (A) airframe, (C) control surfaces and (P) aero-propulsive aerodynamic interaction and (G) due to gravity.

$$m(\dot{\mathbf{V}} + \mathbf{\Omega} \times \mathbf{V}) = \mathbf{F}^{A} + \mathbf{F}^{C} + \mathbf{F}^{P} + \mathbf{F}^{G}. \tag{1}$$

The rotational equations of motion in the body reference frame are:

$$\dot{\mathbf{H}} + \mathbf{\Omega} \times \mathbf{H} = \mathbf{M}^{A} + \mathbf{M}^{C} + \mathbf{M}^{P}. \tag{2}$$

The total angular momentum consists of the 'rigid-body' and 'deformation' component (i.e. in this case, the contribution of the rotors to the angular momentum), as described by Etkin [31], and given as:

$$\mathbf{H} = \mathbf{I}\mathbf{\Omega} + \mathbf{H}^{*}. \tag{3}$$

The 'deformation' component in (3) is then given by the angular momentum of the propellers, which is defined as:

$$\mathbf{H}^{*} = \sum_{k=1}^{n_{\text{prop}}} (I_{\text{prop}} n_{k} \mathbf{i}). \tag{4}$$

Combining Eqs. 2 and 3, the rotational equations of motions can be expanded:

$$\mathbf{I}\dot{\mathbf{\Omega}} + \mathbf{\Omega} \times (\mathbf{I}\mathbf{\Omega} + \mathbf{H}^{*}) + \dot{\mathbf{H}}^{*} = \mathbf{M}^{A} + \mathbf{M}^{C} + \mathbf{M}^{P}. \tag{5}$$

Rearranging Eqs. 1 and 5 yields a set of equations that govern the motion of the aircraft within the flight dynamics model:

$$\dot{\mathbf{V}} = 1/m(\mathbf{F}^{A} + \mathbf{F}^{C} + \mathbf{F}^{P} + \mathbf{F}^{G}) - \mathbf{\Omega} \times \mathbf{V}, \tag{6}$$

$$\dot{\mathbf{\Omega}} = \mathbf{I}^{-1}(\mathbf{M}^{A} + \mathbf{M}^{C} + \mathbf{M}^{P} - \dot{\mathbf{H}}^{*} - \mathbf{\Omega} \times (\mathbf{I}\mathbf{\Omega} + \mathbf{H}^{*})). \tag{7}$$

2.4 Framework requirements

To summarise, a framework adopting this methodology thus requires at least means of generating rudimentary 3D CAD geometry for use in the aerodynamic analysis. The use of panel methods requires a way of geometric modeling that is flexible (parametrised) and of sufficient quality for aerodynamic analysis (i.e. continuous curves with, preferably, nurbs representation). The propeller geometry for the BEM analysis at least requires the definition of 2D airfoil sections along spanwise
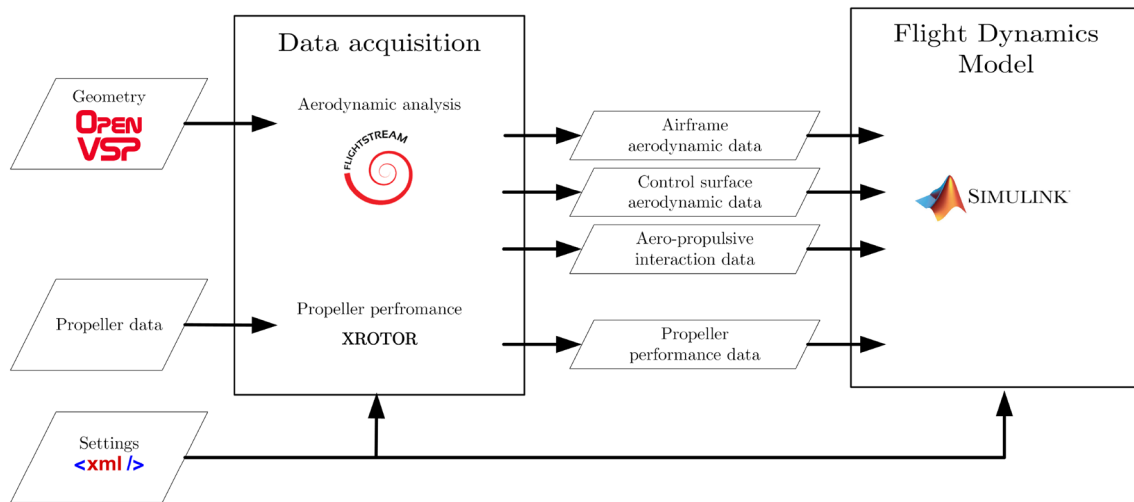
Fig. 4 Overall system architecture of the implemented framework that predicts the dynamic response of aircraft with distributed propulsion, including aero-propulsive interactions

stations of the propeller blade. An absolute minimum is three stations, but more are recommended (10 + stations).

For the data acquisition, a framework that couples an aerodynamic analysis of the airframe with a propeller performance analysis is required. The aerodynamic analysis should at least consist of a potential flow method with viscous correction, i.e. using a surface vorticity solver, and must be capable of incorporating aero-propulsive interactions and evaluating control surface deflections. The propeller performance analysis can be performed through BEM code. The framework also requires the capability to analyse variable geometry and variable number/locations of propulsors. Additionally, all should be coupled to a flight dynamics model (non-linear six-degrees-of-freedom) to analyse aircraft dynamic response, including a (set of) controller(s). The actual framework implementation used in this article will be discussed in the next Sect. 3.

3 Overall framework implementation

The implementation of this framework has been made using parametric MATLAB[3] routines that are able to gather the performance data for any aircraft geometry with any number of propulsors, ensuring reusability in a future design framework. The data acquisition module requires the geometry of the aircraft, which is generated using OpenVSP (Vehicle Sketch Pad).[4] OpenVSP is chosen because of its direct coupling to the chosen surface vorticity solver: FlightStream.[5]

This, commercially available, surface vorticity solver is capable of analysing three-dimensional geometries, while also allowing to model aero-propulsive interactions of propellers on the wing, required for the assessment of minimum control speed condition (i.e. a power-on conditions). This can be done using an unsteady solver where propeller geometry can be modeled in a rotating reference frame or, as used in this work, using a steady solver with actuator disk models for the propellers. The actuator disk inside the surface vorticity solver is modeled using the analytical solutions for actuator disks with variable radial load distribution by Conway [32]. The solver also contains models for flow separation and boundary layer models for the viscous drag components. The propeller performance data are determined using XROTOR,[6] this data provides the input (C_T, collected at some V_∞, radius and rpm) to the actuator disk models inside FlightStream. Torque generated by the propellers is at this stage neglected as its impact is considered small compared to the roll dynamics due to asymmetric lift augmentation. XROTOR is based on blade-element/vortex formulation. This program is used with a prescribed propeller geometry, which is analysed for an advance ratio and inflow velocity to obtain the thrust coefficient.

Figure 4 shows the overall system architecture, all elements will be discussed in more detail in the following subsections. The data acquisition module generates the airframe aerodynamic, aero-propulsive interactions, and control surface deflection data. The airframe aerodynamic data contains the forces and moments created by the airframe. The

---

Table 1 Summary of the performance data gathered by the data acquisition module for the case study aircraft described in Sect. 5

Data		Dep. variables	Indep. variables
Airframe[a]		$C_{0_{x,y,z}}^{A}, C_{M_{0_{x,y,z}}}^{A}$	α, β^{c}
		$C_{p_{x,y,z}}^{A}, C_{M_{p_{x,y,z}}}^{A}$	p^{c}
		$C_{q_{x,y,z}}^{A}, C_{M_{q_{x,y,z}}}^{A}$	q^{c}
		$C_{r_{x,y,z}}^{A}, C_{M_{r_{x,y,z}}}^{A}$	r^{c}
Aero-propulsive[a,c]	Propulsor 1	$C_{1_{x,y,z}}^{P}, C_{M_{1_{x,y,z}}}^{P}$	α, β, C_{T}
	.		
	Propulsor 6	$C_{6_{x,y,z}}^{P}, C_{M_{6_{x,y,z}}}^{P}$	α, β, C_{T}
Control surfaces[a]	Aileron	$\dfrac{\partial C_{x,y,z}^{C}}{\partial \delta_{a}}, \dfrac{\partial C_{M_{x,y,z}}^{C}}{\partial \delta_{a}}$	
	Elevator	$\dfrac{\partial C_{x,y,z}^{C}}{\partial \delta_{e}}, \dfrac{\partial C_{M_{x,y,z}}^{C}}{\partial \delta_{e}}$	
	Rudder	$\dfrac{\partial C_{x,y,z}^{C}}{\partial \delta_{r}}, \dfrac{\partial C_{M_{x,y,z}}^{C}}{\partial \delta_{r}}$	
Propeller[b]		C_{T}, C_{Q}	J

[a]Gathered using FlightStream

[b]Gathered using XROTOR

[c]The aircraft is symmetric, thus data are mirrored

forces and moments created directly by the propulsors and the aero-propulsive interactions are contained in the aero-propulsive interaction data. The forces and moments created by the aileron, elevator, and rudder deflections are captured in the control surface aerodynamic data. Additionally, the data acquisition module requires propeller data containing the two-dimensional airfoil aerodynamic data of the propeller blade sections. These data are used to generate the propeller performance data, which is used in the flight dynamics model to link the propeller performance and the electric engine model. The flight dynamics model takes the performance data as an input to evaluate the flight dynamics of the differential thrust aircraft.

The next subsections detail the two main components of the framework implementation; (1) the data acquisition and (2) the flight dynamics model.

3.1 Data acquisition

The data acquisition module contains two external software tools: FlightStream surface vorticity solver for the airframe, aero-propulsive, and control surface data, and XROTOR for the propeller performance data. Validation studies were performed to determine the suitability of FlightStream; these will be elaborated in Sect. 4. Table 1 summarises the performance data gathered by the data acquisition module.

3.1.1 Airframe aerodynamic data

The airframe aerodynamic data contain the forces and moments created by the non-blown airframe, i.e. clean airframe without any aero-propulsive interactions.[7] Data are gathered for a range of angle of attack (α), sideslip (β), and angular velocities (p, q, r). The forces and moments are interpolated in the flight dynamics model, and can be expressed by Eqs. 8 and 9.

$$C_{x,y,z}^{A} = C_{0_{x,y,z}}^{A}(\alpha, \beta) + \sum_{\omega=p,q,r} C_{\omega_{x,y,z}}^{A}(\omega), \tag{8}$$

$$C_{M_{x,y,z}}^{A} = C_{M_{0_{x,y,z}}}^{A}(\alpha, \beta) + \sum_{\omega=p,q,r} C_{M_{\omega_{x,y,z}}}^{A}(\omega). \tag{9}$$

3.1.2 Aero-propulsive interaction data

Aero-propulsive interaction data contain the forces and moments created by both the propulsors themselves and the aero-propulsive interactions. The data are gathered independently for each propulsor and a superposition principle is assumed in the flight dynamics model. In other words, it is assumed that the aero-propulsive interactions of each propulsor are independent of other propulsors and can be superimposed on a propeller-off aircraft. The assumption is not entirely justified as especially the power augmented lift is dependent also on the neighbouring propulsors (note, this does not refer to propeller–propeller interaction but to the region behind one propeller being affected by the neighbouring propellers). The impact will be elaborated further in Sect. 4.3. Additionally, it should be noted that a possible change in local angle of attack due to failed propulsors is not modeled. The aero-propulsive data are dependent on angle of attack, side-slip, velocity, propeller thrust coefficient and propeller rotational speed, and can be expressed by Eq. 10.

$$(\alpha, \beta, V_{\infty}, n, C_{T}) \underset{\text{FlightStream}}{\mapsto} (C_{x,y,z}^{P}, C_{M_{x,y,z}}^{P}). \tag{10}$$

The aero-propulsive interaction data are collected for angle of attack, side-slip and advance ratio. Velocity is excluded as the aero-propulsive effects are considered as deltas calculated through an actuator disk model that is theoretically inviscid and hence velocity independent. Airframe flow, however, is not. This is expressed by Eq. 11, as opposed to Eq. 10 for the airframe. Only fixed-pitch propellers are considered and hence the advance ratio maps directly to thrust

---

[7] The important aspect of a blown wing is the increase in maximum lift coefficient; the effect generated by the propellers is captured by the aero-propulsive interaction data and added separately as a delta (see also Eq. 1).
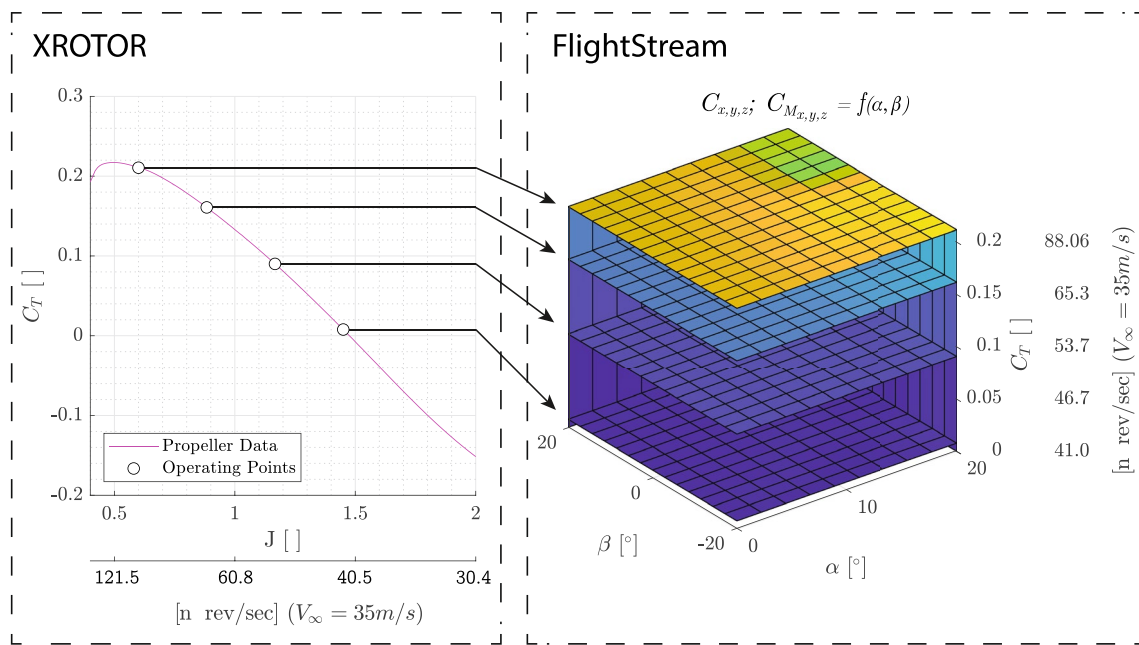
Fig. 5 Operating points and corresponding response surfaces stacked into aero-propulsive interaction data, note the sliding scale for number of revolutions, n

coefficient (note that inside FlightStream a different definition than Eq. 13 is used). Aero-propulsive interaction data influences forces and moments, as indicated in Table 1 and Eqs. 14 and 15, and is combined with airframe, control and gravity forces according to Eq. 1.

$$(\alpha, \beta, n, J \underset{C_{\mathrm{T}}\text{-chart}}{\mapsto} C_{\mathrm{T}}) \underset{\text{FlightStream}}{\mapsto} (C_{x,y,z}^{\mathrm{P}}, C_{M_{x,y,z}}^{\mathrm{P}}), \tag{11}$$

$$n = \frac{V_\infty}{J \cdot d}, \tag{12}$$

$$C_{\mathrm{T}} = \frac{T}{\rho \cdot n^2 \cdot d^4}. \tag{13}$$

Figure 5 shows a visualisation of the aero-propulsive data acquisition. It can be seen that a set of 'operating points' are selected from the thrust chart for the given range of advance ratios. For each operating point, aero-propulsive interaction data are gathered for a range of angle of attack and sideslip. The propeller-off case is subtracted from each result, hence resulting in a dataset containing an approximation of aero-propulsive effects. Finally, the data for each operating point is stacked into a cube. Note that the z-axis in the data cube could be interpreted as advance ratio, since the thrust coefficient and advance ratio are directly linked. The aero-propulsive interaction cubes are interpolated in the flight dynamics module and are expressed by Eqs. 14 and 15.

$$C_{x,y,z}^{\mathrm{P}} = \sum_{i=1}^{n_{\mathrm{props}}} C_{i_{x,y,z}}^{\mathrm{P}}(\alpha, \beta, C_{\mathrm{T}}(J)), \tag{14}$$

$$C_{M_{x,y,z}}^{\mathrm{P}} = \sum_{i=1}^{n_{\mathrm{props}}} C_{M_{i_{x,y,z}}}^{\mathrm{P}}(\alpha, \beta, C_{\mathrm{T}}(J)). \tag{15}$$

3.1.3 Control surface aerodynamic data

The control surface aerodynamic data captures the forces and moment created by the aileron, elevator, and rudder deflections. The data contains a simple derivative. It was not seen necessary to gather any higher dimensional data, as the absolute deflections of the control surfaces are of less importance. Only the relative changes in the deflections are of interest. Additionally, no attempt on investigating aileron/elevator performance or controllers on differential thrust aircraft is made. Therefore, a simple derivative is considered sufficient to represent the forces and moment created by the control surfaces. The forces and moment created by the control surfaces can be expressed by Eqs. 16 and 17.

$$C_{x,y,z}^{\mathrm{C}} = \frac{\partial C_{x,y,z}^{\mathrm{C}}}{\partial \delta_a} \delta_a + \frac{\partial C_{x,y,z}^{\mathrm{C}}}{\partial \delta_e} \delta_e + \frac{\partial C_{x,y,z}^{\mathrm{C}}}{\partial \delta_r} \delta_r, \tag{16}$$
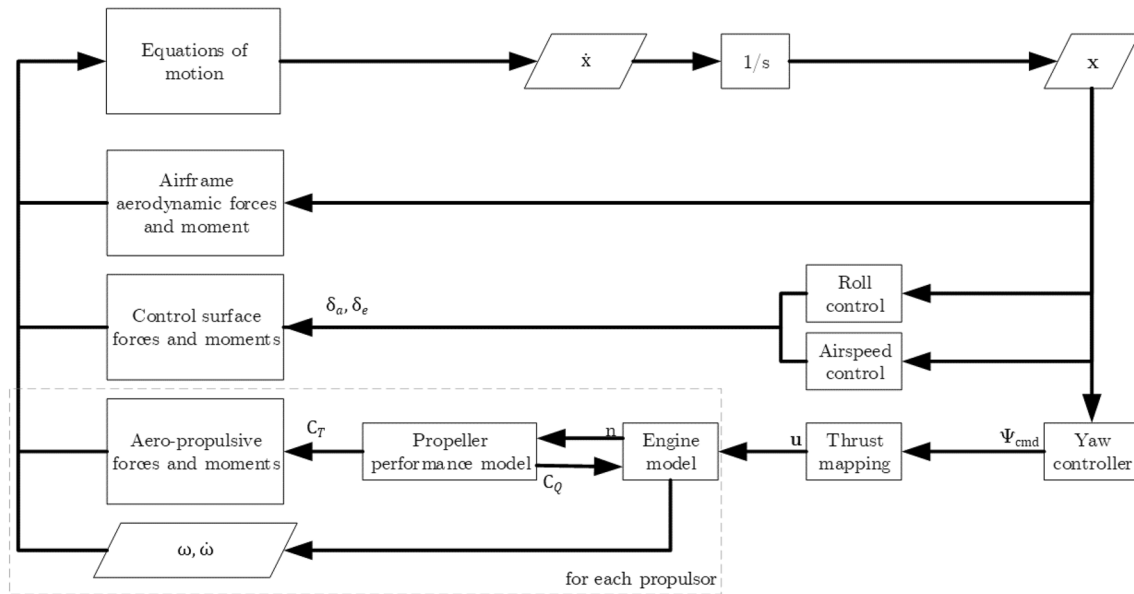
Fig. 6 Overall layout of the flight dynamics model

$$C_{M_{x,y,z}}^{C} = \frac{\partial C_{M_{x,y,z}}^{C}}{\partial \delta_a} \delta_a + \frac{\partial C_{M_{x,y,z}}^{C}}{\partial \delta_e} \delta_e + \frac{\partial C_{M_{x,y,z}}^{C}}{\partial \delta_r} \delta_r. \qquad (17)$$

3.2 Flight dynamics model

The flight dynamics model is the second major component of the overall framework and it is explained in more detail in this section. Figure 6 shows the overall architecture of the flight dynamics model used in this work. The model is created in a Simulink[8] environment.

3.2.1 Control forces

The model assumes a superposition principle, where the forces and moments by airframe, control surfaces, and propulsion are evaluated in separate modules and summed. In other words, the forces and moments contributions of control surfaces and propellers are added to those of the airframe. In an analysis by Huber et al. [30], the super position principle is applied to control surfaces of a delta-wing, where it is concluded that it captures dominant effects but not all couplings and interactions of neighbouring control surfaces. Though the current airframe application is very different, this provides confidence that the followed approach is able to predict the main effects. The propellers, through an actuator disk model, can be considered to create control forces

as well. Although their aerodynamic interaction effect on the wing is included in the current analysis, their impact on aileron effectiveness is not considered. The controllers are implemented using PID controllers and their purpose is to achieve the desired flightpath; to this end, roll and airspeed commands are driving these controllers (aileron and elevator, respectively). The roll control uses a second order model with natural frequency of two and perfect damping, with a rate limit of 1 rad/s.

The effects of control surface deflections and aero-propulsive interactions are each determined with respect to a baseline model. Hence, deltas with respect to the airframe are determined, though coupled effects are not visible. The interactions of different propulsors on each other is (similar to the control surfaces) not taken into account. Additionally, induced velocities on the wing would depend on neighbouring propellers as well. Such effects tend to diminish at approximately one diameter away in spanwise direction. Hence, in this particular model an error is introduced, generally causing an under-prediction of the thrust-induced lift. As such, consequences of sudden thrust-dependent lift loss due to failure of propulsors are even on the conservative side.[9] This will be elaborated further in Sect. 4.3.

---

9 Electric motors, depending on the type used, can be momentarily overloaded in a so-called burst mode providing more than nominal power. However, this is not modeled here and hence results should be treated as indicative in case a burst mode is not available.
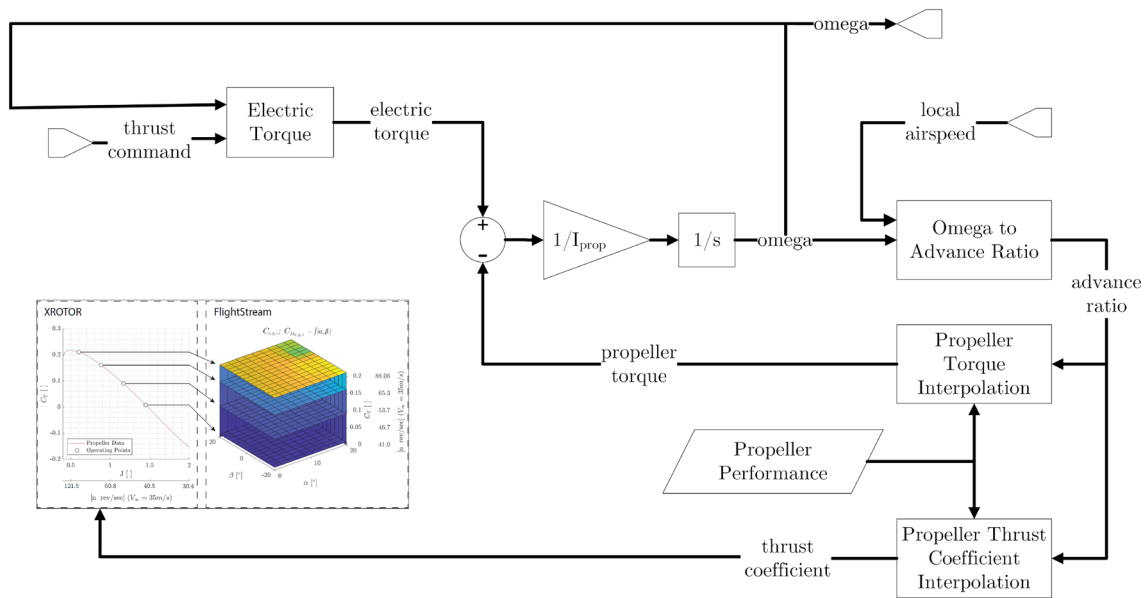
Fig. 7 System diagram for the electric engine model

3.2.2 Engine model

The electric engines used in the flight dynamics model are assumed to operate in a fixed reference frame, with the propulsors modelled independently and producing thrust and rotating fully independently as well. The rotational speed and rotational acceleration is monitored and fed to the equations of motion model, where each propulsor receives the "local velocity" independently. Note that roll rate and local up-wash of the wing is not assumed to impact local velocity. Also the angle of attack of the propeller is not impacting propeller performance. The engine model is frictionless and is governed by Eq. 18.

$$\dot{\omega} \cdot I_{\text{prop}} = T_{\text{m}} - T_{\text{p}}. \tag{18}$$

Here, $\dot{\Omega}$ is the propeller shaft acceleration, I_{prop} is the propeller inertia, T_{m} the torque created by the electric motor (data taken from the Maxwell X-57 [33]) and T_{p} the torque created by the propeller. Since the aero-propulsive modelling is only able to analyse positive thrust coefficient (C_{T}), the thrust and moment for negative C_{T} are used according to Eqs. 19 and 20, relating to propeller diameter (D), revolutions (n), density (ρ) and distance of the propeller axis to the body axis (l). Thus, in the case of negative thrust coefficients, aero-propulsive interactions are ignored.

if $C_{\text{T}} < 0$ then:
$$F_x^{\text{P}} = C_{\text{T}} \cdot \rho \cdot n^2 \cdot D^4, \tag{19}$$
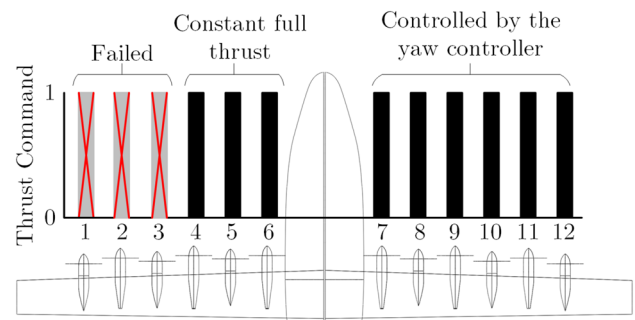

Fig. 8 Illustration of the inoperative propulsors, constant full-thrust propulsors and propulsors for directional control

$$M_z^{\text{P}} = F_x^{\text{P}} \cdot l. \tag{20}$$

Figure 7 shows the system diagram for the model. The engine model takes as an input the thrust command and outputs rotational speed and thrust coefficient. Within the model, thrust command is converted into an electrical torque. The propeller imposes an opposing torque, which is interpolated from the propeller performance data. The local airspeed refers to the axial velocity at the propeller.

3.2.3 Directional control under inoperative conditions

The directional control of the aircraft can be achieved by altering the power of the propulsors in addition to rudder deflection. Figure 8 illustrates the approach that is followed for differential thrust under inoperative conditions. The operative propulsors on the inoperative wing (i.e. on the
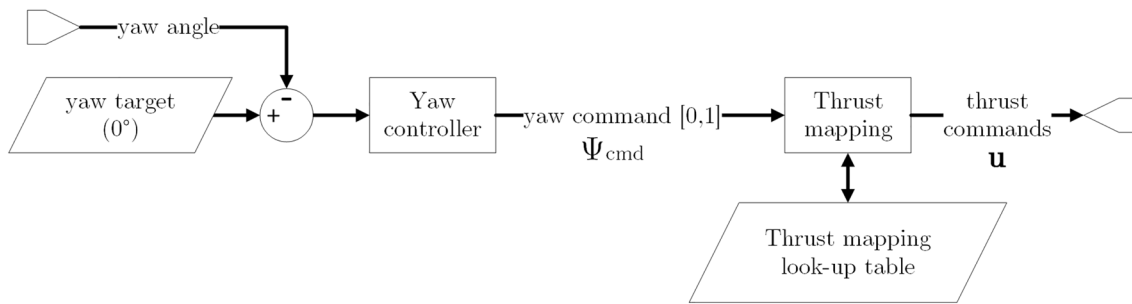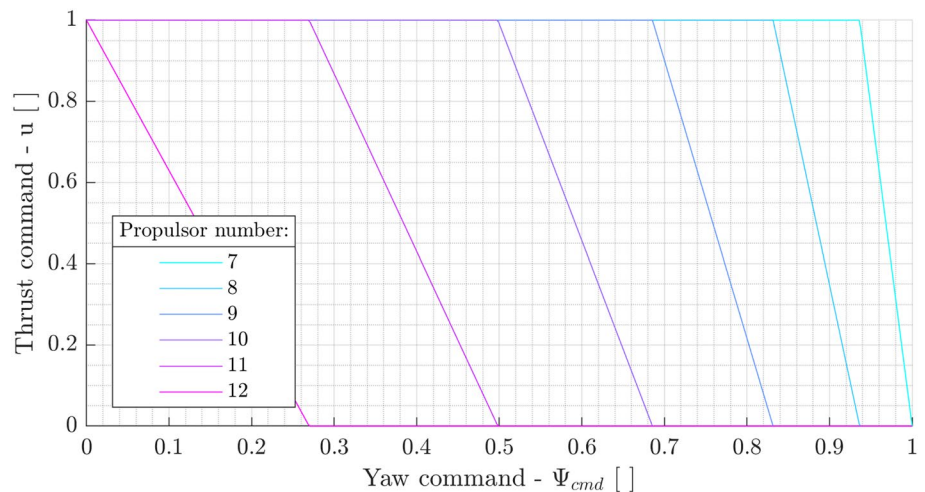
Fig. 9 System diagram of the yaw control and thrust mapping

Fig. 10 Thrust mappings of the case study aircraft. Outboard propulsors [1, 3] have failed, [4, 6] maintain full thrust, and propulsors [7, 12] (inboard to outboard) are controlled by the yaw controller

wing where three propulsors fail) maintain full thrust, and are therefore not controlled. This was decided because the inoperative condition requires maximum power throughout the recovery manoeuvre, and to simplify the analysis.

The directional control is implemented by a yaw controller, which controls the overall yawing effort. The controller outputs a yaw command, which is converted to individual thrust commands by thrust mapping. Figure 9 shows the system diagram for yaw control and thrust mapping. The yaw controller is a hand-tuned PID ($P = 3, I = 0.2, D = 14$) controller converting the error (mismatch) in yaw angle to a required yaw command. Hand tuning was done to mimic the behaviour of a potential directional controller.

The yaw command is in the range from zero to one. It is defined that yaw command of zero equals a full thrust on all of the propulsors on the operative wing, and yaw command of one equals that all of the propulsors on the operative wing are turned off. Indeed the range should be minus one to one to have yawing in both directions, yet here only an engine inoperative scenario is studied for one side. To decide how the propulsors are operated when the yaw command is

between minimum and maximum, a thrust distribution or mapping of the thrust requirement to the different propulsors is required. It should be noted that absolute available/required thrust must be used for control of the flight path.

The thrust mappings are stored as a look-up table and interpolated in the flight dynamics model. Figure 10 shows the thrust mapping for the case study aircraft. It can be seen that the thrust mapping, logically, favours the outermost propulsors for creating yawing moment. (Similar to Kou et al. [27], where also the outboard controllers are prioritised by the yaw command though with a much more sophisticated control scheme). This is because the outermost propulsors have the largest moment arm; therefore, reducing their thrust results in the highest available thrust, whilst simultaneously satisfying a specific yaw command.[10]

---

[10] An axis prioritisation study was outside the scope of this work. However, as illustrated, reducing the outer propulsors will always provide the largest possible yawing moment whilst maintaining the highest possible thrust (to have the highest possible lift augmentation). The maximisation of remaining thrust is only intended for the case study presented here and would not directly apply in other flight phases that were outside the scope of this work.
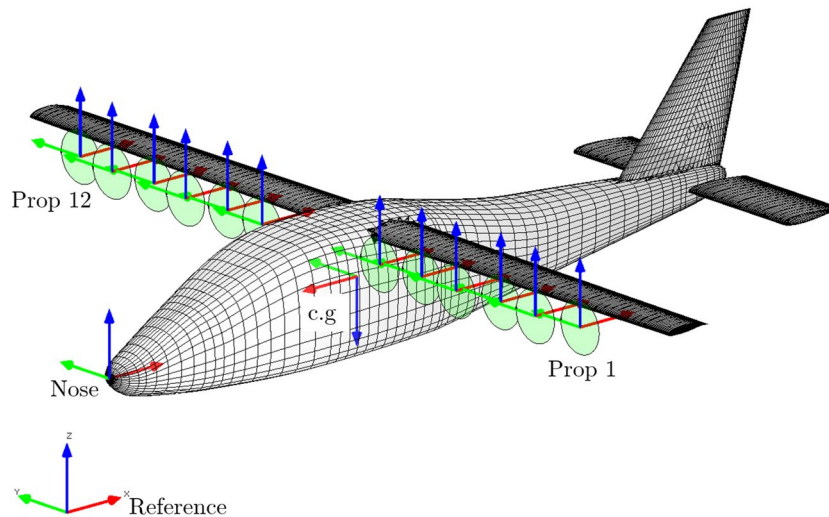
Fig. 11 The case study aircraft X-57Mod geometry

4 Validation and verification

Two validation studies were performed for the aerodynamic analysis: validation of the external aerodynamic forces and moments, and validation of the aero-propulsive interactions. Also, an investigation was performed regarding the performance of the developed methodology in terms of the superposition principle of the aero-propulsive interactions.

4.1 Unpowered X-57 Maxwell

A validation study was performed to validate the external aerodynamic forces and moments of the surface vorticity solver. The results are compared against two Reynolds-averaged Navier Stokes (RANS) flow solvers that have been used on the X-57 Maxwell[34], the STAR-CCM+ unstructured solver, and the Launch Ascent Vehicle Aerodynamics (LAVA) structured curvilinear flow solver. The X-57 geometry used here is publicly available in the OpenVSP hangar.[11] The geometry is modified for usage with FlightStream by sharpening the blunt trailing edges, skewing the upper and lower surfaces.

In addition, a simplified version of the X-57, referred to as X-57Mod (more details in Sect. 5), is studied. The geometry is presented in Fig. 11. The case study aircraft contains 12 fixed pitch high-lift propulsors. The X-57Mod is tailored to suit the data acquisition purposes by reducing the complexity of the geometry. The simplifications include the removal of the nacelles, pylons, and landing gear fairings. Additionally, the vertical tailplane is simplified, and the horizontal tailplane split to allow easy deflection of the surface.

Figure 12 shows the lift, drag, rolling moment, pitching moment, and yawing moment coefficients of the geometries.

It can be seen that FlightStream is predicting the overall trends quite well, with some under prediction of drag (post-stall) and over prediction of lift especially for the original X-57 geometry. For that specific study, also the lift curve slope is over predicted. However, the results do start to differ more at the high angles of attack, which is likely caused by the analysis entering the stall region, and the surface-vorticity solver not being able to capture the more subtle flow phenomena. The rolling moment is captured with good accuracy. The pitching moment though is not captured accurately, with the pitch break not being captured. Although, for both the FlightStream analyses, the pitch-curve slope is captured fairly well.

Overall, the software performs on the level that is expected from a mid-fidelity level software. The results do indicate that actual numerical values have to be treated carefully, but the trends are captured sufficiently to perform a comparative study as intended by this research. Especially, post-stall behaviour is not captured sufficiently accurately. However, this region is not of interest for the power-on studies (performed at speeds 5m/s or more higher than the stall speed of 29.8m/s of the X-57[12]).

4.2 Aero-propulsive interactions

Another validation study was performed for the aero-propulsive interactions. For these studies, wind tunnel measurements and geometry from Sinnige et al. [35] are used for comparison. These include a conventional wing-mounted configuration (Fig. 13), with a spanwise location as seen in typical propeller aircraft, and a wing tip mounted
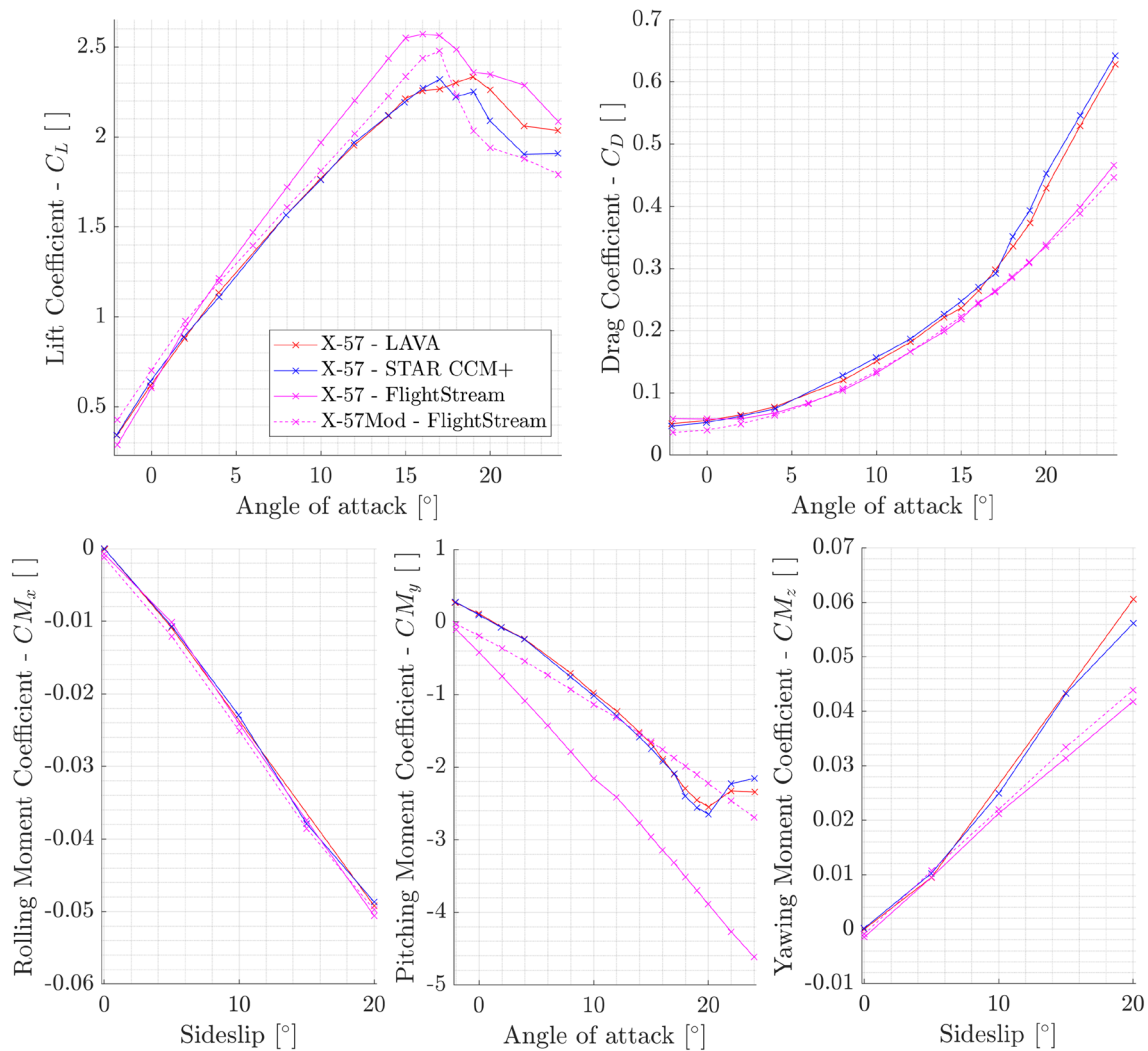

Fig. 12 Lift, drag, and pitching moment coefficients versus angle of attack and rolling, and yawing moment coefficients versus sideslip angle for X-57 in FlightStream, compared to RANS

configuration (Fig. 13). Both studies use the same wing, nacelle, and propeller, though installed at different spanwise locations. The test data does not include wind tunnel wall corrections. Hence, the inner tunnel wall of the TU Delft Low Turbulence Tunnel[13] is also modelled. The propeller itself is modelled as an actuator disk inside the panel code (FlightStream). Figure 14 illustrates the model of the conventionally mounted configuration with a wind tunnel wall.

It was noted that the flow behaviour in the case of the wing-tip mounted propeller with nacelle is erroneous in the surface vorticity solver. In the case of the wing-tip mounted propeller, the wake of the wing was not correctly attaching to the nacelle, and the location of the wing-tip vortex

was thus misaligned. Due to this misalignment, the wing-tip study was performed by removing the nacelle from the geometry, which resulted in a much more accurate location of the wing-tip vortex. Hence, nacelles were also removed from the case study treated in Sects. 5 and 6.

Figure 15 shows the lift-drag polars of the configurations. The lift coefficient is agreeing well, though with a small over-prediction of drag for the same lift coefficient. Here, thrust producing cases are modelled, where the errors are larger at lower advance ratio (higher thrust settings). In the case of the wingtip-mounted propeller, the shape of the drag polar is more skewed, which is partially attributed to the removal of the nacelle.

Overall, it can be said that the results are within the accuracy expected for the level of fidelity. It gives sufficient confidence to use this software for the research presented in this article. The power augmented lift is captured well for the

---

[13] https://www.tudelft.nl/lr/organisatie/afdelingen/aerodynamics-wind-energy-flight-performance-and-propulsion/facilities/low-speed-wind-tunnels/low-turbulence-tunnel.
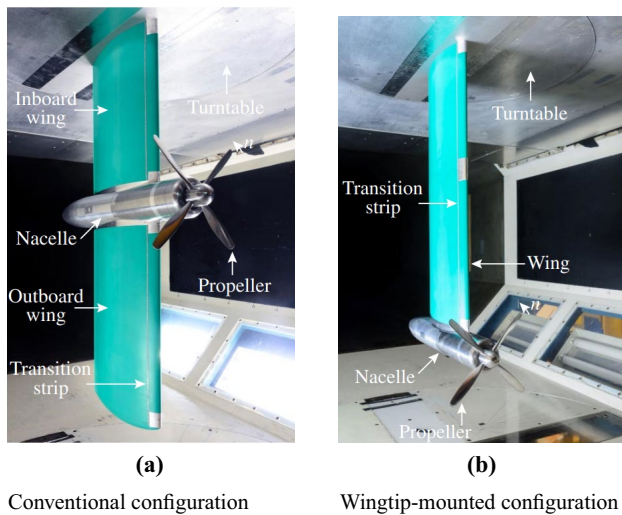
(a) Conventional configuration   **(b)** Wingtip-mounted configuration

Fig. 13 The conventional and the wing-tip configuration used in the study from Sinnige et al. [35] (images courtesy of Dr. T. Sinnige)

conventionally mounted case, with decent drag prediction and all necessary trends are captured as well.

4.3 Impact of superposition principle

A verification study was performed to investigate the impact of the superposition principle of the aero-propulsive results. The superpositioned aero-propulsive results interpolated from the data cubes are compared against direct results, i.e.

without interpolation or superposition of the interaction data as described Sect. in 3.1.2 on the prop-off wing. The comparison data are gathered for the case study aircraft with all 12 propulsors installed. The propeller advance ratio is 0.6, representative for high trust setting, highlighting worst-case performance (in terms of power-augmented lift differential). This case study is also representative in terms of conditions evaluated during the minimum control speed assessment presented later.

Table 2 shows the errors of the superpositioned aero-propulsive data compared against direct results of a full model with all 12 propellers on the aircraft. It can be seen that the superposition principle holds well for C_x^P and $C_{M_y}^P$ with a mean absolute error of 2.0% and 3.6% respectively. However, in the case of C_z, the mean absolute error is 24.6%. In conclusion the superposition principle cannot be justified for an assessment of the magnitude of power-augmented lift. In fact, the datacube approach gives a fairly constant underestimation of C_z (around 0.25). This is likely attributed to the close proximity of neighbouring propellers and the effects on induced velocities on the wing behind. Alternatively, RSM techniques could be employed to improve the datacube.

However, considering the computational advantage in the current framework, the approach is still used here as it does capture the aero-propulsive interactions and is illustrative of the general trends. Actually, the underprediction applies for all data points showing a difference that is always in the order of 0.25. It should be noted though that C_z results are
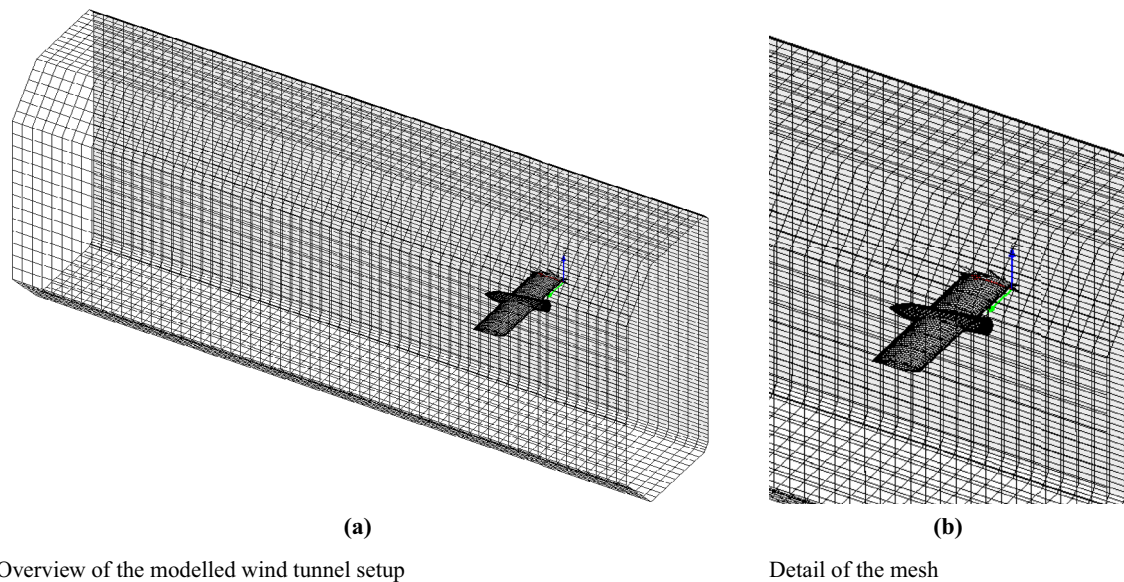

(a) Overview of the modelled wind tunnel setup   **(b)** Detail of the mesh

Fig. 14 FlightStream mesh of the conventionally mounted configuration with a wind tunnel wall
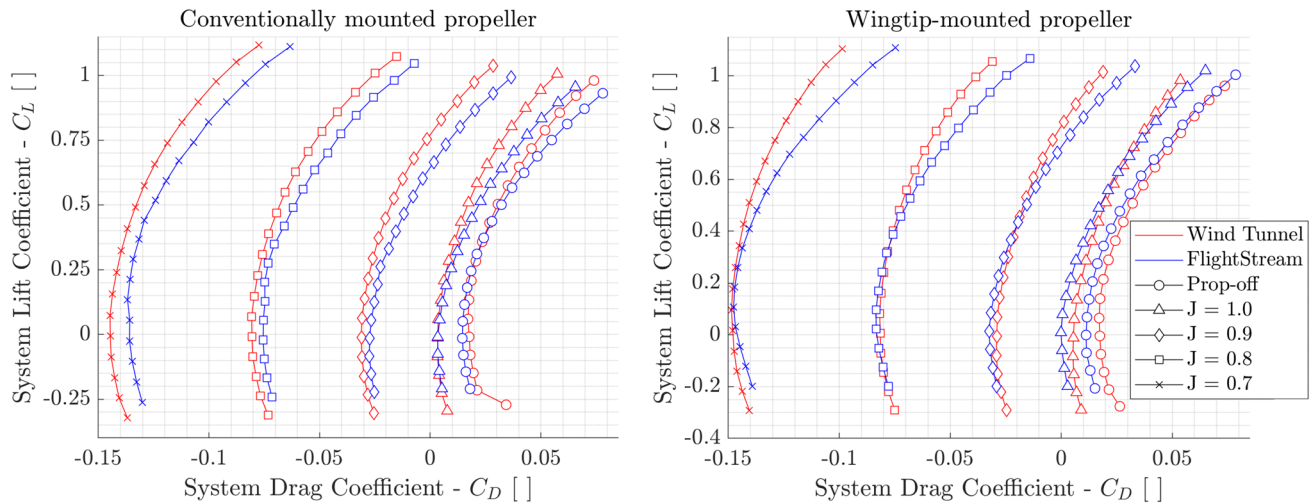
Fig. 15 System lift-drag polar of the wing, propeller and nacelle (wind tunnel data from [35]). Note that for the wingtip-mounted case, the wingtip nacelle is removed from the FlightStream model

Table 2 Error of the aeropropulsive interactions for the data cube interpolation (superposition principle) compared against direct FlightStream results

α [°]	β [°]	FlightStream			Data cube			Error (%)		
		C_x^P	C_z^P	$C_{M_y}^P$	C_x^P	C_z^P	$C_{M_y}^P$	C_x^P	C_z^P	$C_{M_y}^P$
5	0	0.76	− 0.79	− 0.53	0.76	− 0.54	− 0.51	− 0.37	− 31.68	− 3.04
10	0	0.83	− 1.03	− 0.61	0.81	− 0.77	− 0.57	− 1.96	− 24.60	− 6.23
15	0	0.87	− 1.02	− 0.73	0.86	− 0.89	− 0.68	− 1.61	− 12.21	− 7.68
5	5	0.76	− 0.77	− 0.52	0.76	− 0.53	− 0.52	− 0.43	− 30.28	− 0.70
10	5	0.83	− 1.02	− 0.61	0.81	− 0.77	− 0.58	− 2.30	− 25.29	− 5.20
15	5	0.88	− 1.06	− 0.74	0.83	− 0.77	− 0.68	− − 6.61	− 26.80	− 7.80
5	10	0.76	− 0.74	− 0.55	0.77	− 0.52	− 0.57	0.25	− 29.41	3.40
10	10	0.83	− 0.98	− 0.65	0.81	− 0.74	− 0.64	− 2.05	− 24.49	− 1.47
15	10	0.86	− 0.98	− 0.80	0.84	− 0.70	− 0.75	− 2.15	− 28.41	− 7.21
5	20	0.79	− 0.76	− 0.76	0.77	− 0.54	− 0.77	− 1.76	− 28.25	1.49
10	20	0.83	− 0.91	− 0.77	0.80	− 0.66	− 0.74	− 3.35	− 28.03	− 3.04
15	20	0.84	− 0.89	− 0.95	0.79	− 0.62	− 0.84	− 5.12	− 30.19	− 11.15

$J = 0.6, V_\infty = 35$ m/s

$C_T = 0.2106, n = 101.3$ rev/s

Table 3 X-57Mod. case study parameters

Variable	Value	Unit
Reference area	6.194	m^2
Reference chord	0.643	m
Reference span	7.099	m
Mass	1180	kg
I_x	1617	kg m^2
$I_{xy} = I_{xz} = I_{yz}$	0	kg m^2
I_y	1927	kg m^2
I_z	2931	kg m^2

Table 4 Case study propulsion parameters

Variable	Value
Number of propulsors	12
Number of blades	3
Spin direction	Inboard-up
Blade pitch angle	30°
Diameter	0.576 m
Motor torque	24 Nm
RPM range for torque	2000–5450 RPM [33]
Propulsor total inertia	0.0069 kg m^2

likely underpredicted and, hence, effects as described later would in fact be further aggravated (loss of lift).

5 Case study setup

The case study under consideration in this article is the loss of three adjacent propulsors on the outer-most part of the wing, to assess the effects of distributed propulsion under engine inoperative conditions. This section describes the setup for this case study, as well as the requirements enforced on the flight condition under consideration. For this case study, the modified version of the NASA X-57 Maxwell is used as described before. Table 3 shows the main parameters of the aircraft. The case study aircraft contains 12 fixed pitch high-lift propulsors. The electrical engine torque curve of the motors is provided by [33]. Table 4 summarises the propulsion parameters, the propeller geometry is based on that of the XPROP propeller.[14]

The flight dynamic simulations start from a trimmed steady state with a minimum control speed (V_{MC}) of 35 m/s and maximum thrust for all propulsors. The selected minimum control speed is 1.13 times the maximum thrust stall speed of 31 m/s. The engine inoperative condition begins at $t = 1$ s, when three propulsors on the left wing become inoperative. This is the same conditions as studied by [19]. The loss of three propellers is hypothesised for the abrupt failure of one propeller damaging its two neighbours, with the outboard ones having the largest moment arm to the aircraft center of gravity, therefore causing the most adverse yawing condition. Failed propulsors are assumed to be windmilling, with windmilling drag asserted instantly at $t = 1$ s. Or, in other words, the propulsors state is then changed from thrust to windmilling drag.

After a specified response time, the system is allowed to react to the engine inoperative condition. It is highlighted that before this response time is reached all aircraft controls remain inactive (i.e. the aircraft is not allowed to respond). The response time simulates delays in the system, for example fault identification time, processing time, motor response time (inertia is modelled), etc. The selection of the response time is an important decision that directly impacts the performance of the recovery manoeuvre. In the study by Wortmann [19], the response time is set to one second. However, it was quickly seen that the aircraft is not recoverable with one second response time. It is argued that the lack of aero-propulsive interactions in the Wortmann's study results in significantly different results. However, it is important to note that Wortmann investigated the PT2006T aircraft, with different wing geometry then X-57 (though it is based on the same aircraft), and hence the results are not directly
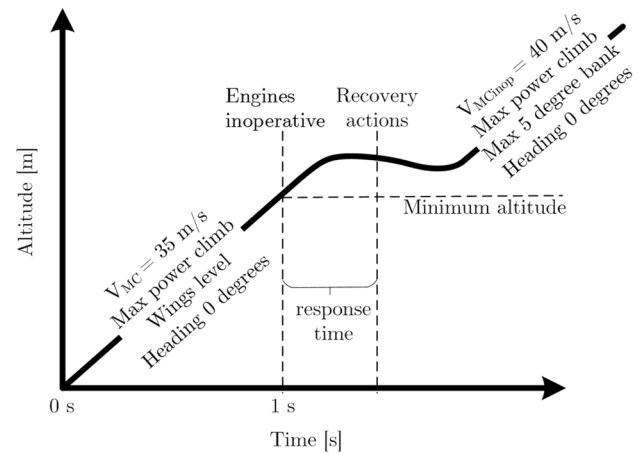

Fig. 16 Summary of the case study setup

comparable. Considering that a response time of one second yielded non-recoverable failures, and it is expected that the system can react faster, a response time of half a second is suggested. The impact of response time is investigated in Sect. 6.3, where response time is varied between 200 and 800 ms.

The engine inoperative condition causes a loss in power augmented lift, hence requiring the powered stall speed and minimum control speed to be increased. The stall speed in this case is dependent on the thrust mapping, and the number and location of the failed propulsors. Consequently, the aircraft must accelerate during the recovery manoeuvre to prevent a stall. The minimum inoperative control speed ($V_{MC_{inop}}$) is selected to be 40 m/s (1.13 times the new stall speed).

The requirements for the recovery manoeuvre emanate from the European Aviation Safety Agency (EASA) CS-23 regulations.[15] The regulations are adapted to suit the differential thrust aircraft study and are summarised below. Figure 16 summarises and illustrates the case study setup.

– Aircraft must be able to accelerate from V_{MC} to $V_{MC_{inop}}$
– Bank angle is not allowed to be more than 5°
– Maximum heading change of the aircraft must remain below 20°
– Altitude during the entire recovery manoeuvre must be above the initial inoperative altitude
– Steady state climb gradient must be above 2%

---

[14] ae.tudelft.nl/propellerdata.

[15] Certification Specifications for Normal-Category Aeroplanes (CS-23), Amendment 5, European Aviation Safety Agency (EASA), 2017.
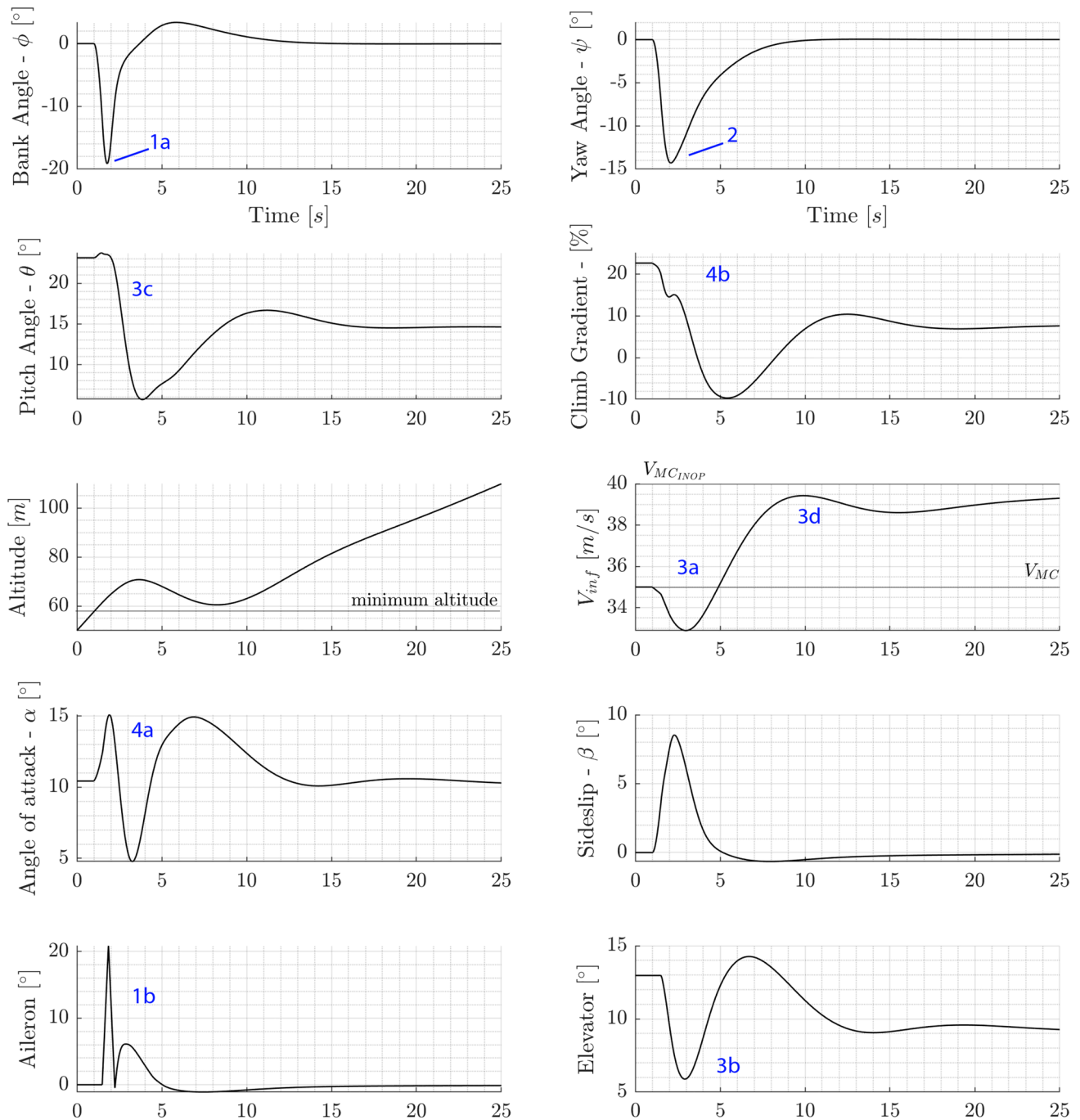
Fig. 17 The overall aircraft performance during the recovery manoeuvre

6 Case study results

The conceptual design phase in aircraft design typically includes an analysis of critical conditions for the sizing for control and stability, to determine the necessary horizontal and vertical tail sizes (as for example in the method by [36]). As such, the previously described framework is applied to an investigation under engine inoperative conditions at minimum control speed, for a representative case study with distributed electric propulsion leveraging power-augmented lift. As a worst-case scenario, the failure of the three outermost propellers is considered. This section presents the results of the assessments of the general characteristics under these inoperative conditions, the impact of differential thrust versus rudder only for yaw-authority, and
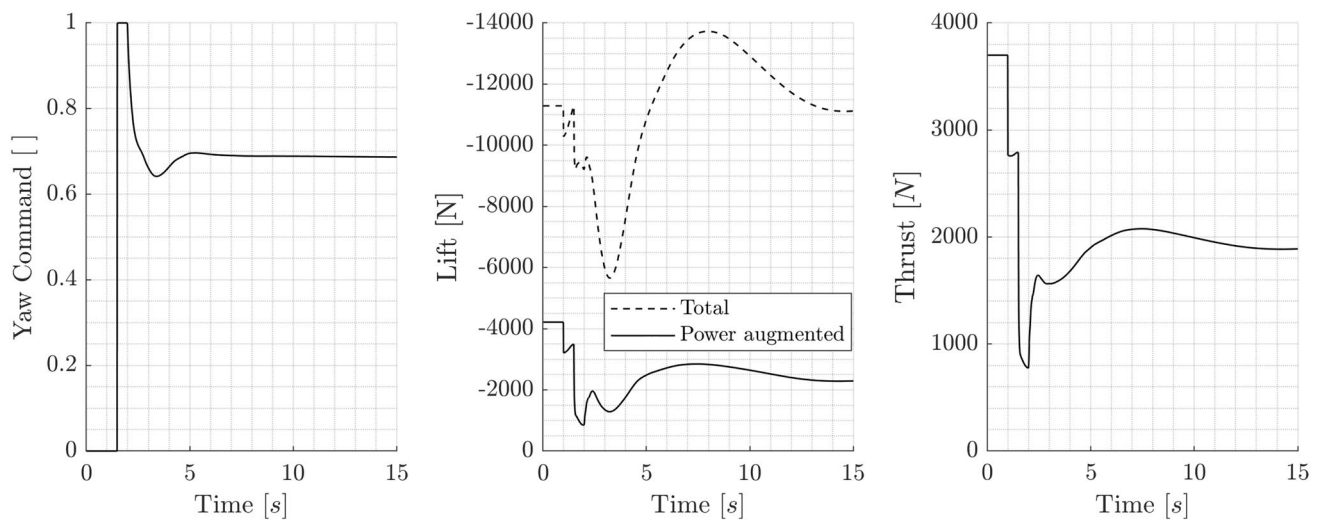
Fig. 18 The yaw command (as defined in Sect. 3.2.3), lift, and thrust during the recovery manoeuvre; NB lift is facing upwards, hence a negative force in the reference frame
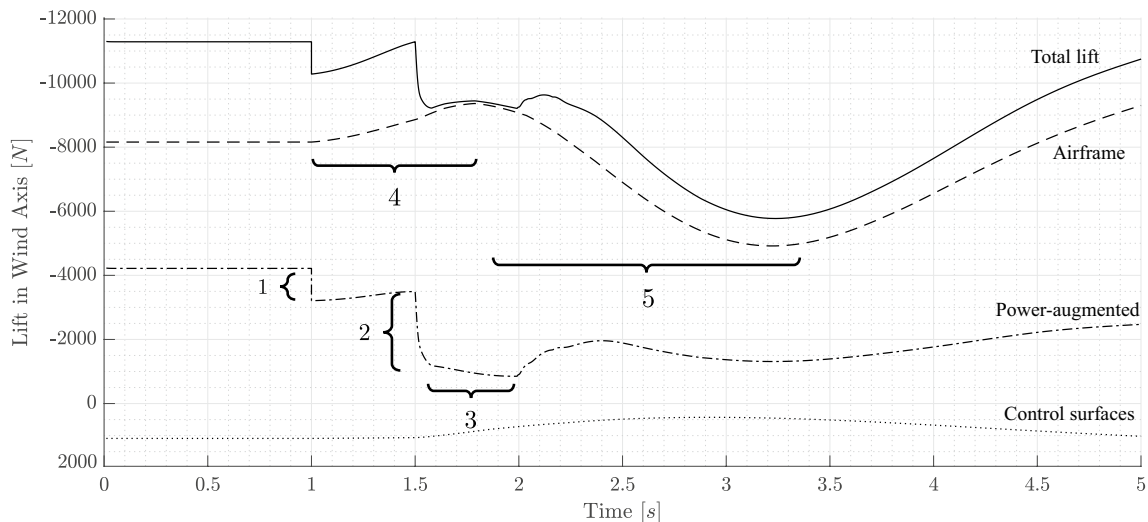
Fig. 19 Lift sources of the aircraft during the first five seconds of the simulation

the impact of vertical tailplane size reduction in relation to response time. The latter, i.e. vertical tail reduction, is often advocated as a potential benefit of distributed propulsion, where a reduction of vertical tail size is expected to result in a drag and weight benefit.

6.1 General characteristics

The goal of this study is to examine the general characteristics of differential thrust under engine inoperative conditions. The response time is set to 500 ms and thrust mapping as described in Sect. 3.2.3 is applied. Figure 17 shows the

overall aircraft performance during the recovery manoeuvre. In general, the inoperative conditions results in a relatively aggressive manoeuvre, which is, however, recovered relatively quickly. More details on the behaviour are presented in Figs. 18 and 19. Several observations can be made from the figure:

1. The bank angle is rapidly increasing after the engine inoperative condition (1a). This is mainly due to the asymmetric power augmented lift, but also due to the rolling moment caused by the vertical tailplane. After the 500 ms response time, the aileron autopilot (1b) is rapidly correcting for the increased bank angle and the bank angle peaks at 19°, after which it returns to zero.

2. The yaw angle (2) is also increasing rapidly after the inoperative condition. The differential thrust is reacting to the increased yaw angle after the response time and the yaw angle peaks at 14.2°.

3. The velocity of the aircraft is rapidly reducing after the engine inoperative condition (3a). The elevator autopilot (3b) is reacting to the speed reduction by commanding the aircraft to pitch down. The pitch down (3c) reduces the angle of attack and stops the reduction in velocity. As the aircraft starts to regain velocity (3d), the elevator starts to pitch the nose up, and the climb gradient returns to positive. Note that after the engine inoperative condition the elevator autopilot is targeting a new $V_{MC_{inop}}$ velocity of 40 m/s due to the increased stall speed (i.e. again 1.13 times the new stall speed).

4. The angle of attack is rapidly increasing after the engine inoperative conditions (4a). This is due to the reduction in power augmented lift which results in reduction in climb gradient (4b), as well as change in pitching moment due to a change in thrust causing a slight increase in pitch angle. The angle of attack is rapidly reduced due to the elevator autopilot control effort to prevent the reduction in the velocity. The angle of attack is increased again when the elevator autopilot is commanding to pitch up as the new target airspeed is approaching. It is important to note that the elevator autopilot is not responding to the angle of attack, but to the airspeed instead. However, the reaction to reach the new inoperative condition minimum control speed results in the prevention of stall, which would otherwise occur in case the aircraft would be to maintain the initial minimum control speed.

Figure 18 shows the yaw command, lift, and thrust during the recovery manoeuvre. It can be seen that the power augmented lift provides 37% of the total lift at the initial conditions. Changes in lift during the recovery are further detailed in Fig. 19 (numbers in the following text refer to labeled elements in this figure). After the engine inoperative condition, there is an immediate reduction in the power augmented lift (delta lift due to propulsors) due to the failed propulsors (1). The power augmented lift reduction results directly in 8.9% reduction in total lift. Also, the thrust is reduced due to the failed propulsors by 25%. After the response time the yaw controller is reacting to the yaw condition (2) and the yaw command is momentarily saturated (3). During the saturation all of the propulsors of the operative wing are turned off to reduce the yaw effort. Hence, the power augmented lift is further reduced by the yaw control effort. It can be seen that the reduction in the power augmented lift is significant due to the yaw control effort. It can also be observed that the thrust is drastically reduced. Comparing to the operative

condition, thrust is reduced by 79% momentarily. After the saturation, power augmented lift and thrust are increased. The increased airframe lift due to increased angle of attack immediately after the inoperative conditions is visible in (4). The discussed behaviour results in both reduction of climb gradient due to the reduced lift, as well as increase of bank angle due to the rolling moment caused by the asymmetric lift. The reduction in thrust is resulting in a reduction of velocity which results in the temporary altitude reduction, due to the elevator autopilot targeting the new increased minimum control speed to prevent stall (5).

In conclusion, the recovery manoeuvre presents new challenges for differential thrust aircraft as significant parts of thrust and power augmented lift are lost during the recovery manoeuvre. This causes the aircraft to enter into close proximity of stall. Additionally, the airspeed is reducing due to the significant loss in thrust, which requires rapid actions from the elevator autopilot. This causes the aircraft to temporarily descent during the recovery manoeuvre. As C_z is likely underpredicted, these results would be further amplified in case the superposition principle for aero-propulsive deltas is replaced by a direct computation.

6.2 Rudder replacement

Another analysis has been performed where the performance of differential thrust is compared to a traditional rudder for yaw authority under engine inoperative conditions at a minimum control speed climb. Rudder deflection is limited to 45°, and the maximum deflection rate is set to 2 rad/s. Note that in the case where only the rudder is used, all of the operating propulsors remain at full thrust to maintain as much airspeed as possible and continue the climb. Differential thrust is operated using the previously presented mapping to provide a yaw command. The response time is set to 500 ms for both differential thrust and rudder-only case.

Figure 20 shows the overall performance of the differential thrust and rudder case. It can be seen that the performance of the rudder is not satisfying requirements, as the yaw angle cannot be contained within the required 20° limit. The rudder is not able to provide sufficient countering yawing moment to compensate for the adverse yawing moment caused by the failure of three propulsors on one side. In addition, during the recovery manoeuvre, the case with rudder-only attains dangerous bank angles. This is mainly due to the asymmetric power augmented lift that is present in this case, indicating that, on the fully operative side, propellers should not be run at full throttle. Note that in the case of differential thrust there also exists a momentary asymmetric power augmented lift, which is, however, compensated by the yaw control effort which reduces power of the propulsors on the operative wing, hence stabilising the
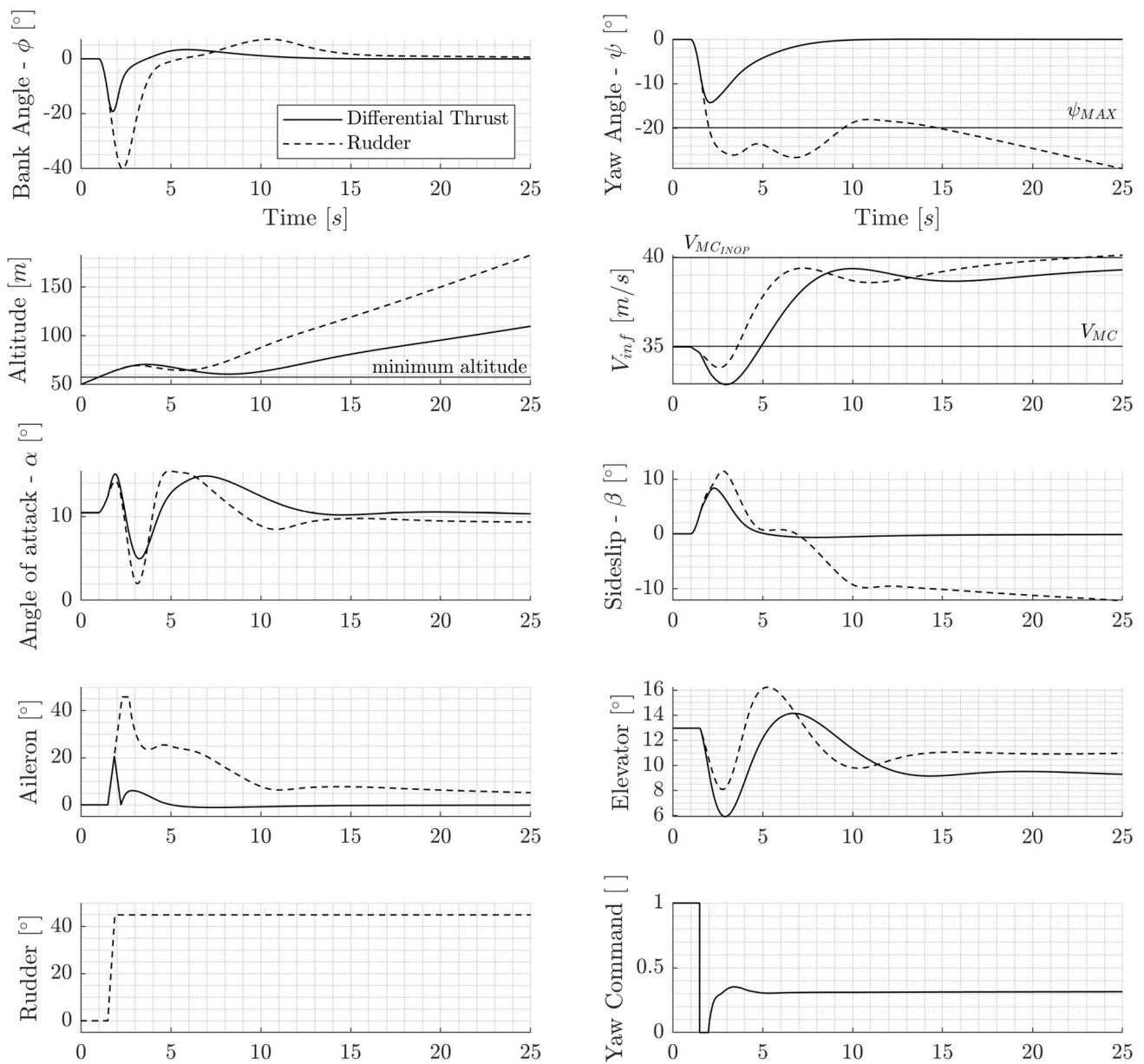
Fig. 20 The overall performance of the differential thrust and rudder-only cases for yaw authority

power augmented lift. This can also be observed from the aileron deflection, as the rudder-only case requires constant aileron deflection to maintain zero bank angle. The rolling moment of the rudder-only case is further aggravated by the rolling moment caused by the deflected rudder.

Naturally, the climb performance of the aircraft only using the rudder is significantly better compared to the case with differential thrust, because all the operating propellers are remaining at full power. The steady-state climb gradient of the rudder-only case is 13.24% and for differential thrust 8.10%. However, in order for the rudder case to satisfy the yaw angle requirements, the power of the operative

propulsors must also be reduced and therefore the climb gradient would also reduce.

In conclusion, the differential thrust provides a significant amount of yaw authority. In the case study, the differential thrust performed superior over the rudder-only case, as the rudder is not able to satisfy the requirements due to the lack of yaw authority. The challenge of differential thrust is the altitude reduction and rapid change in bank angle due to the significant reduction in thrust and power augmented lift. Also, the climb gradient is reduced due to the yaw control effort compared to the rudder case. Altogether, for the case study aircraft the differential thrust can fully replace the
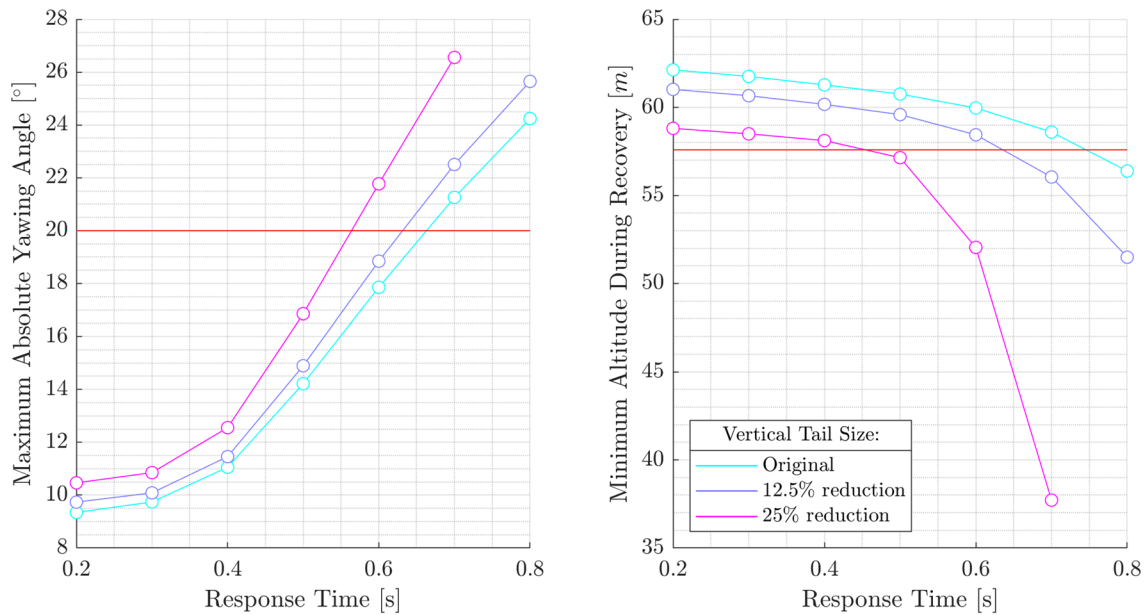
Fig. 21 The maximum absolute yawing angle and minimum altitude during recovery for the reduced vertical tailplanes as a function of response time

rudder for the climb condition that was studied, and is seen even as a necessity, with further options for improvement by combining both.

6.3 Vertical tailplane area reduction

The final analysis presented here assesses the potential for a possible reduction of the vertical tailplane. The assessment is performed for the same failure case, with original, 12.5% reduced, and 25% reduced vertical tailplane area. Additionally, the impact of the response time on the recovery performance is investigated. The response is varied in the range of 200–800 ms to illustrate its impact. In both cases, differential thrust is used.

Figure 21 shows the absolute maximum yawing angle and the minimum altitude during the recovery manoeuvre. The red horizontal line on the maximum absolute yawing angle figure shows the 20° requirement limit. The yaw angle is not allowed to exceed this limit. The red horizontal line on the minimum altitude figure shows the initial altitude at inoperative condition. The aircraft is not allowed to descent below this altitude during the recovery manoeuvre. It can be seen that in the case of 400 ms response time, all of the vertical tailplane sizes still satisfy the requirements. However, at 700 ms, only the original rudder still meets the requirements and 800 ms results in a failure of any of the vertical tail sizes to satisfy the requirements.

It can therefore be concluded that the response time of the differential thrust has a significant impact on the overall performance of the recovery manoeuvre. It can be seen that

a reduction of the vertical tailplane is possible as long as the response time of the system is sufficiently low.

7 Conclusions

This paper presented an assessment of flight dynamics and control under engine inoperative conditions for aircraft with distributed electric propulsion, using differential thrust. The assessment included aero-propulsive interaction effects and was performed during a climb at minimum control speed. The developed methodology allows the data acquisition of the aerodynamic performance of an aircraft, including aero-propulsive effects, and the evaluation of the flight dynamic performance under engine inoperative conditions.

The engine inoperative condition presents a challenging condition for differential thrust aircraft. The aircraft experiences a significant and abrupt loss in thrust and power augmented lift, which is caused by the failed propulsors and the yaw control effort required by the operative propulsors. The reduction in thrust is directly reducing the velocity of the aircraft. Additionally, the loss of power augmented lift increases the aircraft stall speed and part of the still available thrust is required for yaw control, hence cannot be used to accelerate. Consequently, it is necessary to increase the velocity in order to prevent aircraft from entering into a stall during the recovery manoeuvre. This results in a temporary reduction in altitude during the recovery manoeuvre. Results show that during the recovery manoeuvre, the aircraft experiences a 78% reduction

in total thrust and 30% reduction in total lift caused by the aggressive yaw control effort required to control the heading of the aircraft.

The aero-propulsive effects contribute significantly to the recovery manoeuvre during the engine inoperative conditions for aircraft leveraging power augmented lift. It was seen that at minimum control speed a significant portion (37%) of the lift is provided by the power augmented lift, before failure. During the engine inoperative condition, the reduction in power augmented lift is contributing both to the rolling moment and temporary altitude reduction during the recovery manoeuvre, resulting in only half of the power-augmented lift after recovery. It must be noted that with the implemented model, the power-augmented lift is actually underestimated. This indicates that the effects are likely even more pronounced.

Differential thrust can be seen to replace the performance of the rudder. Differential thrust provides a significant amount of yaw authority during the engine inoperative condition and is able to counter the adverse yawing moment caused by the inoperative propulsors. It was seen that a rudder as an only source of directional control was not able to provide enough yaw authority for the case study aircraft for full power on the propulsors. Additionally, the asymmetric power augmented lift after the failure causes a constant and significant rolling moment as all the operative propulsors maintain full thrust. This rolling moment is counterbalanced in the case of differential thrust aircraft due to the yaw control effort reducing the thrust on the operative wing propulsors. The rolling moment is directly impacting the maximum bank angle during the recovery manoeuvre, and in the rudder case the aircraft encountered dangerous bank angles. The main challenge of differential thrust is the reduced thrust and power augment lift due to the yaw control effort, which reduces the aircraft climb gradient and adversely impacts the recovery manoeuvre.

The effects of vertical tail size were shown in relation to the response time, which was shown to have a significant impact on the recovery performance. An analysis of the achievable reduction was not performed and would require more realistic flight controllers and a more detailed investigation. The method allows future investigation of arbitrary geometries and arbitrary number of propulsors, as well as investigation of other flight phases (e.g. approach and crosswind landing), although it is recommended to further improve the data-cube interpolation of aero-propulsive interaction data, as well as the integration of angle of the flow at the propeller, to account for angle of attack effects of the propellers. An appropriately designed and integrated controller should be considered early on in the (conceptual) design of distributed propulsion aircraft, as the actual controller will have a significant impact on the performance of such vehicles that rely on (coupled) power-augmented lift and active differential thrust. Additionally, instead of using a fixed reaction time for the complete control system, using modelled actuator dynamics may suffice along with correcting the thrust mapping after a defined failure-detection time. For future work, it may also be interesting to perform a bandwidth test of propeller motor combination to model the expected performance.

References

1. European Commission and Directorate-General for Mobility and Transport and Directorate-General for Research and Innovation, Flightpath 2050 : Europe's vision for aviation : maintaining global leadership and serving society's needs, Publications Office, 2011, https://doi.org/10.2777/50266

2. Felder, James L. (NASA Glenn Research Center Cleveland, OH United States), Presentation, EnergyTech 2015 (Cleveland, OH), Work of the US Gov. Public Use Permitted, GRC-E-DAA-TN28410, WBS: WBS 081876.02.03.30.01,November 30, 2015, https://ntrs.nasa.gov/citations/20160009274

3. Borer, N.K., Patterson, M.D., Viken, J.K., Moore, M.D., Clarke, S., Redifer, M.E., Christie, R.J., Stoll, A. ., Dubois, A., Bevirt, J.B., Gibson, A.R., Foster, T.J., Osterkamp, P.G.: Design and performance of the NASA SCEPTOR distributed electric propulsion flight demonstrator. In :Proceedings of the 16th AIAA Aviation Technology, Integration, and Operations Conference, Washington, DC, USA. American Institute of Aeronautics and Astronautics (2016)

4. Antcliff, K.R., Capristan, F.M., Conceptual design of the parallel electric-gas architecture with synergistic utilization scheme (PEGASUS) concept. In: 18th AIAA/ISSMO Multidisciplinary Analysis and Optimization Conference, p. 4001 (2017)

5. Rothaar, P.M., Murphy, P.C., Bacon, B.J., Gregory, I.M., Grauer, J.A., Busan, R.C., Croom, M.A.: NASA langley distributed propulsion VTOL tilt-wing aircraft testing, modeling, simulation, control, and flight test development. In: Proceedings of the 14th AIAA Aviation Technology, Integration, and Operations Conference, Atlanta, GA, USA. American Institute of Aeronautics and Astronautics (2014)

6. Schiltgen, B.T., Freeman, J.: Aeropropulsive interaction and thermal system integration within the ECO-150: a turboelectric distributed propulsion airliner with conventional electric machines. In: 16th AIAA Aviation Technology, Integration, and Operations Conference, p. 4064 (2016)

7. Hermetz, J., Ridel, M., Döll, C.: Distributed electric propulsion for small business aircraft: a concept-plane for key-technologies investigations. In: Proceedings of the 30th Congress of the International Council of the Aeronautical Sciences, Daejeon, South Korea. International Council of the Aeronautical Sciences (2016)

8. Stoll, A.M., Mikić, G.V.: Design studies of thin-haul commuter aircraft with distributed electric propulsion. In: Proceedings of the 16th AIAA Aviation Technology, Integration and Operations Conference, Washington, DC, USA. American Institute of Aeronautics and Astronautics (2016)

9. Jansen, R.H., Bowman, C., Jankovsky, A., Dyson, R., Felder, J.: Overview of NASA electrified aircraft propulsion research for large subsonic transports. In: *Proceedings of the 53rd AIAA/SAE/ASEE Joint Propulsion Conference, Atlanta, GA, USA*. American Institute of Aeronautics and Astronautics (2017)

10. Kim, H.D., Perry, A.T., Ansell, P.J.: A review of distributed electric propulsion concepts for air vehicle technology. In: AIAA/IEEE Electric Aircraft Technologies Symposium (EATS), vol. 2018, pp. 1–21. IEEE (2018). https://doi.org/10.2514/6.2018-4998

11. Sgueglia, A., Schmollgruber, P., Bartoli, N., Atinault, O., Benard, E., Morlier, J.: Exploration and sizing of a large passenger aircraft with distributed ducted electric fans. In: 2018 AIAA Aerospace Sciences Meeting, p. 1745 (2018)

12. Steiner, H.J., Seitz, A., Wieczorek, K., Plötner, K., Iskiveren, A.T., Hornung, M.: Multi-disciplinary design and feasibility study of distributed propulsion systems. In: Proceedings of the 28th ICAS Congress, Brisbane, Australia. International Council of the Aeronautical Sciences (2012)

13. de Vries, R., Hoogreef, M.F.M., Vos, R.: Preliminary sizing of a hybrid-electric passenger aircraft featuring over-the-wing distributed-propulsion. In: AIAA Scitech 2019 Forum (2019)

14. Hoogreef, M.F.M., de Vries, R., Sinnige, T., Vos, R.: Synthesis of aero-propulsive interaction studies applied to conceptual hybrid-electric aircraft design. In: AIAA Scitech,: Forum. Orlando, Florida, USA (2020). https://doi.org/10.2514/6.2020-0503

15. "Clean Aviation Joint Undertaking" (corporate author), Strategic Research and Innovation Agenda, Bruxelles, Belgium, July 2020, updated December 2021.

16. Moore, M.D.: Misconceptions of electric aircraft and their emerging aviation markets. In: 52nd Aerospace Sciences Meeting, p. 0535 (2014). https://doi.org/10.2514/6.2014-0535

17. Stoll, A.M., Bevirt, J., Moore, M.D., Fredericks, W.J., Borer, N.K.: Drag reduction through distributed electric propulsion. In: 14th AIAA Aviation Technology, Integration, and Operations Conference, p. 2851 (2014). https://doi.org/10.2514/6.2014-2851

18. Schiltgen, B.T., Freeman, J.: ECO-150-300 design and performance: a tube-and-wing distributed electric propulsion airliner. In: AIAA Scitech 2019 Forum, p. 1808 (2019)

19. Wortmann, G.: Investigating the dynamic response of hybrid-electric propulsion systems for flight control application. Ph.D. thesis, Technische Universität München (2016)

20. Brelje, B.J., Martins, J.R.: Electric, hybrid, and turboelectric fixed-wing aircraft: a review of concepts, models, and design approaches. Progr. Aerosp. Sci. **104**, 1–19 (2019). https://doi.org/10.1016/j.paerosci.2018.06.004

21. Freeman, J.L., Klunk, G.T.: Dynamic Flight simulation of spanwise distributed electric propulsion for directional control authority. In: AIAA/IEEE Electric Aircraft Technologies Symposium (EATS), vol. 2018, pp. 1–15. IEEE (2018). https://doi.org/10.2514/6.2018-4997

22. Klunk, G.T., Freeman, J.L., Schiltgen, B.T.: Tail area reduction for aircraft with spanwise distributed electric propulsion. In: AIAA/IEEE Electric Aircraft Technologies Symposium (EATS), vol. 2018, pp. 1–13. IEEE (2018). https://doi.org/10.2514/6.2018-5022

23. Pfeifle, O., Frangenberg, M., Notter, S., Denzel, J., Bergmann, D., Schneider, J., Scholz, W., Fichter, W., Strohmayer, A.: Distributed electric propulsion for yaw control: testbeds, control approach, and flight testing. In: AIAA AVIATION 2021 FORUM (2021). https://doi.org/10.2514/6.2021-3192

24. Nguyen Van, E., Alazard, D., Pastor, P., Döll, C.: Towards an aircraft with reduced lateral static stability using differential thrust. In: 2018 Aviation Technology, Integration, and Operations Conference, p. 3209 (2018a). https://doi.org/10.2514/6.2018-3209

25. Van Nguyen, E., Troillard, P., Jezegou, J., Alazard, D., Pastor, P., Döll, C.: Reduction of vertical tail using differential thrust: influence on flight control and certification. In: AEGATS'18, Toulouse, France, pp. 1–8 (2018)

26. Ciliberti, D., Nicolosi, F., Vecchia, P.: A new approach in aircraft vertical tailplane design. In: 22th AIDAA Conference, Associazione Italiana di Aeronautica e Astronautica Naples (Italy) (2013)

27. Kou, P., Wang, J., Liang, D.: Powered yaw control for distributed electric propulsion aircraft: a model predictive control approach. IEEE Trans. Transport. Electrification **7**, 3006–3020 (2021)

28. Van Nguyen, E., Alazard, D., Döll, C., Pastor, P.: Co-design of aircraft vertical tail and control laws with distributed electric propulsion and flight envelop constraints. CEAS Aeronaut. J. **12**(1), 101–113 (2021). https://doi.org/10.1007/s13272-020-00481-8

29. Soikkeli, J.: Vertical tail reduction through differential thrust: an initial assessment of aero-propulsive effects on lateral-directional stability and control in engine inoperative conditions. Master's thesis, Delft University of Technology (2020). http://resolver.tudelft.nl/uuid:77b54c76-1ab8-4220-a26d-1394b2079849. Accessed 2 Dec 2021

30. Huber, K.C., Vicroy, D.D., Schuette, A., Huebner, A.: UCAV model design and static experimental investigations to estimate control device effectiveness and Stability and Control capabilities. In: 32nd AIAA Applied Aerodynamics Conference. American Institute of Aeronautics and Astronautics (2014). https://doi.org/10.2514/6.2014-2002

31. Etkin, B.: Dynamics of Atmospheric Flight. Courier Corporation, Chelmsford (2012)

32. Conway, J.T.: Analytical solutions for the actuator disk with variable radial distribution of load. J. Fluid Mech. **297**, 327–355 (1995). https://doi.org/10.1017/S0022112095003120. https://www.cambridge.org/core/article/analytical-solutions-for-the-actuator-disk-with-variable-radial-distribution-of-load/DD0A601AF1DF77542B094AF6DDCD99EB

33. Hall, D., Chin, J., Anderson, A., Smith, A., Edwards, R., Duffy, K.P.: Development of a Maxwell X-57 high lift motor reference design. In: AIAA Propulsion and Energy 2019 Forum, p. 4481 (2019). https://doi.org/10.2514/6.2019-4481

34. Yoo, S., Duensing, J.: Computational analysis of the external aerodynamics of the unpowered X-57 Mod-III aircraft. In: AIAA Aviation 2019 Forum, p. 3698 (2019). https://doi.org/10.2514/6.2019-3698

35. Sinnige, T., van Arnhem, N., Stokkermans, T.C., Eitelberg, G., Veldhuis, L.L.: Wingtip-mounted propellers: aerodynamic analysis of interaction effects and comparison with conventional layout. J. Aircr. **56**(1), 295–312 (2018). https://doi.org/10.2514/1.C034978

36. Torenbeek, E.: Synthesis of Subsonic Airplane Design. Delft University Press, Delft (1982)